

Direct numerical simulation of separating turbulent boundary layers

By **Martin Skote** and **Dan S. Henningson**

Dept. of Mechanics, KTH, SE-100 44, Stockholm, Sweden

Direct numerical simulation of two turbulent boundary layer flows has been performed. The boundary layers are both subject to a strong adverse pressure gradient. In one case a separation bubble is created while in the other the boundary layer is everywhere attached. The data from the simulations are used to investigate scaling laws near the wall, a crucial concept in turbulence models. Theoretical work concerning the inner region in a boundary layer under an adverse pressure gradient is reviewed and extended to the case of separation. Excellent agreement between theory and data from the direct numerical simulation is found in the viscous sub-layer, while a qualitative agreement is obtained for the overlap region.

1. Introduction

The separation of boundary layer flow is of crucial importance in many applications, including airfoils, rear windows on cars, and turbine blades. Separation is difficult to predict with current turbulence models, and the design of devices that either lose their functionality or have their optimum performance close to the onset of separation is an engineering difficulty.

A vast number of theoretical and/or experimental work has been presented throughout the last decades, and lately direct numerical simulations (DNS) have become an important tool for further investigation of this type of flows. Although laboratory experimental techniques have improved and the reliability of results from experiments has increased, there is still need for DNS for improving the results in the near-wall region. Also, turbulent structures and the instantaneous flow fields are better analyzed using DNS results.

1.1. Theoretical investigations

In most theoretical investigations of boundary layers it is of crucial importance to determine the relevant velocity scale. For a zero pressure gradient (ZPG) boundary layer such a velocity scale is naturally chosen as the friction velocity,

$$u_\tau \equiv \sqrt{\nu \left. \frac{\partial u}{\partial y} \right|_{y=0}}. \quad (1)$$

However, in the case of a boundary layer under an adverse pressure gradient (APG), u_τ is not the relevant velocity scale. This is true especially for strong APGs and low Reynolds numbers. For a separating boundary layer this is clear since u_τ becomes zero in this case. In a number of studies the case of a strong APG and separation has been investigated theoretically. In many such studies a velocity scale based on the pressure gradient is defined,

$$u_p \equiv \left(\nu \frac{1}{\rho} \frac{dP}{dx} \right)^{1/3}. \quad (2)$$

In an analysis based on u_p , Stratford (1959) obtained a square-root law for the velocity profile from the assumption of zero wall stress and mixing length theory. Townsend (1961) refined the theory based on mixing length to the case of non-zero (but positive) wall shear stress and obtained a law with both square-root and logarithmic parts based on u_τ as a velocity scale. Kader & Yaglom (1978) extended the Stratford velocity profile to the case of positive wall stress. However, they kept the square-root law based on u_p , and let the influence of a non-zero wall shear stress be accounted for by varying the constants. Mellor (1966) arrived at a similar expression as Townsend. The work of Townsend was later reviewed by McDonald (1969) who included non-linear inertia effects in the expression for the velocity profile.

Afzal (1996) obtained similar expressions for the velocity profile as Townsend by using asymptotic matching. Durbin & Belcher (1992) also used asymptotic theory for the analysis of velocity profiles. They obtained a three layer structure of the turbulent boundary layer under an APG. Melnik (1989) also obtained a three layer structure by extending the asymptotic analysis of Yajnik (1970) and Mellor (1972) with an algebraic turbulence model. Skote & Henningson (1999) simplified the formulation of Townsend and showed that the analysis could be valuable for turbulence modelling purposes.

Instead of using u_τ or u_p as the velocity scale and letting the velocity profile depend on the pressure gradient and Reynolds number, some investigators have tried to make the profiles collapse on a single curve in an outer scaling. This seems to be possible only if a velocity scale is determined a posteriori, with the objective to make the profiles collapse. Coles (1956) proposed a wake function to account for the variation of the velocity profile in the outer (or wake) region of the boundary layer. The form of the wake function has later been modified in a number of ways, see e.g. Musker (1979) for further references. Perry & Schofield (1973) and Schofield (1981) used a scaling for the outer part of the velocity profile designed to match the profiles to a half-power law close to the wall. They claimed that the velocity scale is related to the maximum shear stress.

Thus, there are two fundamentally different theoretical approaches to the velocity profile in a turbulent boundary layer under a strong APG. One is focusing on the local pressure gradient as the important parameter determining the shape of the velocity profile, the other is focusing on a velocity scale, defined

through a fitting procedure, that will make the velocity profiles collapse onto a single curve. In this work we will develop further the analysis where the local pressure gradient is the key factor.

1.2. Experiments

Many experiments have been performed on separated flows, albeit most of them consider separation caused by a sharp edge, or an obstacle, see e.g. the review of Simpson (1996) for a collection of references, and the work of Hancock (2000) for references to the latest experiments.

The experiments on separation of a flat plate turbulent boundary layer include the works of Perry & Fairlie (1975), Simpson *et al.* (1977, 1981*a,b*), Dengel & Fernholz (1990), Driver (1991) and Alving & Fernholz (1996, 1995). Some of these investigations have also tried to develop different scalings of the velocity profile in both outer and inner variables.

Simpson *et al.* (1977) showed that the Perry-Schofield scaling is supported upstream of separation, however with the the streamwise derivative of the longitudinal and normal Reynolds stresses included in the estimation of the maximum shear stress. They concluded that the shear stress gradient is less than the streamwise pressure gradient due to the Reynolds stresses and the convective terms in the momentum equation.

Simpson *et al.* (1981*a,b*) developed a scaling based on the maximum back-flow velocity and its distance from the wall for the back-flow profile, which was shown to consist of three layers: the layer closest to the wall which is governed by viscous forces, a relatively flat intermediate layer and the outer back-flow which is dominated by the large-scale outer region flow. No universal 'back-flow function' could be found. Upstream of separation the logarithmic law was valid, as well as the Perry-Schofield scaling for the outer part. As separation is approached the scalings are not fulfilled. Furthermore, they concluded that the velocity profile in the outer part is not described by a universal wake function. The normal and streamwise Reynolds stresses contribute to the turbulence energy production at separation, and the enhanced turbulence energy production in the outer region supply turbulence energy to the back-flow region by turbulent diffusion.

Dengel & Fernholz (1990) performed measurements in an axisymmetric turbulent boundary layer. Three cases were investigated with skin friction zero, slightly negative, and slightly positive. They concluded that the logarithmic law is not valid when the first reverse-flow events occur. Furthermore, the velocity profile does not confirm the Perry-Schofield scaling. Instead they let a seventh order polynomial represent an asymptotic velocity profile close to separation. However, Dengel & Fernholz did not base the velocity scale on the maximum stress. Instead, they obtained the velocity scale by fitting the velocity profiles to a half-power law, as suggested by Schofield (1981). Reynolds stresses increased downstream in all three cases and the turbulence production had its maximum far out in the boundary layer.

Driver (1991) performed measurements on two boundary layers on an axisymmetric body with similar pressure distributions but very different flows. One is attached and the other is separated. He concluded that above a certain value of the pressure gradient (in viscous scaling) the mean flow profile does not obey the law of the wall. The attached boundary layer was found to be in equilibrium and the Clauser parameter was nearly constant.

Alving & Fernholz (1996) performed an experiment on an axisymmetric body with a turbulent boundary layer that separates in a short region. They reported decreased Reynolds stresses in the inner region and large peaks away from the wall. After reattachment, the inner region is slower in its recovery than the outer part and the recovery does not start at the wall. Hence, the large scale structures are intact over the separation bubble and then interact with near-wall flow after reattachment. Alving & Fernholz (1995) investigated the scaling of the velocity profiles from their experiment. They compared the Durbin-Belcher and Perry-Schofield scalings, with the conclusion that the latter works better than the former. However, they did not actually use the velocity scale proposed by Perry & Schofield (1973), but rather determined their velocity scale so that the velocity profiles close to separation collapse with the profile given by Dengel & Fernholz (1990).

The consensus from the experiments mentioned above is that the turbulence is intensified above a separated region while it is decreased in the back-flow itself. Velocity profiles at streamwise positions close to the separation point can only be made to collapse in the outer part by a fitting procedure of the velocity scale. Upstream of separation the experiments give no evidence on how the velocity profiles should be scaled. No universal profile for the back-flow seems to exist and the proper scaling is still an open question.

1.3. *Direct numerical simulations*

A few direct numerical simulations (DNS) of separated turbulent boundary layer flows have been performed earlier.

Na & Moin (1998*a,b*), hereafter abbreviated as NM, used a second-order finite difference method to simulate a turbulent separation bubble. The computational box was $350 \times 64 \times 50$ based on the δ^* at the turbulent inflow. The number of points was $513 \times 193 \times 129$. The inflow condition was taken from Spalart's temporal ZPG simulation. The velocity profiles were neither linear in the viscous sub-layer nor logarithmic further from the wall at all streamwise positions. The location of maximum turbulence intensity occurred above the separation bubble.

The near-wall flow from the simulation by NM has previously been investigated by Skote & Henningson (1999). Good agreement between theory regarding the viscous sub-layer (recapitulated here in section 2.1.1) and DNS data was found in the region just upstream of separation.

Spalart & Coleman (1997), hereafter abbreviated as SC, performed DNS of a separation bubble with heat transfer. They used a spectral code with

$640 \times 200 \times 256$ modes. Their inflow-outflow boundary condition was based on the fringe region technique with a turbulent inflow. Their results showed that separation has large effects on the boundary layer, and that many assumptions which are valid for an attached layer cannot be applied to the separated boundary layer. The Reynolds shear stress increased dramatically over the separation bubble as did the turbulent kinetic energy. This is explained by a lift-up of turbulent fluid from the wall region that weakens the blocking effect of the wall. The increased turbulent energy can also be explained by a contribution from the normal and streamwise Reynolds stresses as argued by SC. Negative production of turbulent kinetic energy was observed in the later part of the separation bubble. This was not further explained by SC but was probably due to a positive Reynolds shear stress in that part of the flow. However, SC recognized that the effect of the rapid distortion on the boundary layer might lead to results which are not valid for turbulent separation bubbles in general.

In both of these simulations the boundary condition on the upper boundary was set by imposing a normal velocity that varies downstream and thus controls the separation bubble. Many results are hence similar for both simulations. The streamwise velocity profiles have a gradient at the upper boundary due to the boundary condition, thus the velocity profiles constitute a boundary layer with no freestream edge, where the streamwise velocity gradient and the normal velocity are small.

Both NM and SC noted that the streaks near the wall are eliminated by an APG. In NM they concluded that the vortical structures are lifted above the bubble and impinge on the wall in the reattachment region.

The simulations performed here are different from the ones by NM and SC in some important aspects. First, the boundary condition used in the present simulations gives a boundary layer with a well defined freestream edge, thus permitting an investigation of integral parameters which was not possible in NM and SC. Second, the separated region is longer than in NM and SC, hence the local distortion of the boundary layer is less severe. The strength of the back-flow is also stronger, which reveals new phenomena.

In this work we start with a review and extension of the theory concerning velocity profiles in an attached and separated turbulent boundary layer in section 2. The results from the simulations are presented in section 3. A presentation of the numerical methodology, including a resolution check, is given in section 3.1. This is followed by a general description of the flow, including both instantaneous structures and turbulence statistics, in section 3.2. The theoretical results from section 2 are compared with DNS data in section 3.3. The results are further discussed in section 4, and comparison with NM and SC will be made, as well as with some experimental data.

In the present work we focus on the near-wall flow since few results from the near-wall region in a separated flow have previously been reported. The flow close to the wall is scrutinized by comparing results from theoretical considerations with data obtained from the DNS

2. The turbulent boundary layer equations

In the past, much effort has been spent to obtain numerically solvable ordinary differential equations for the parameters quantifying the turbulent boundary layer. See e.g. Schlichting (1979), Rotta (1962) and Cebeci & Smith (1974) for references. Using such methods, separation and reattachment can be predicted in some cases. However, no general formula to predict separation has been offered. The emphasis today is shifted towards more general closures of the Navier-Stokes equations, based on turbulence models. Therefore, no attempts to analyze or improve the methods based on simplified versions of the turbulent boundary layer equation (TBLE) are conducted here. The TBLE is used to extend and improve the theoretical understanding of the streamwise velocity profile in the inner region of the turbulent boundary layer.

The near-wall behavior of a turbulent boundary layer close to separation, or fully separated, is difficult to analyze with the TBLE, since a separated flow does not permit the simplifications of the Navier-Stokes equations leading to the TBLE. However, even if the TBLE is not valid when the downstream development of a separating boundary layer is to be calculated, it can still be used to understand what happens locally in the boundary layer.

Results from a straightforward analysis of the TBLE is of importance for the development and calibration of turbulence models. The near-wall laws derived for ZPG boundary layers have been used extensively for obtaining boundary conditions in calculations of boundary layer flow with turbulence models. Thus, better near-wall laws for turbulent boundary layers would improve the predictions made of APG flows using turbulence models. The near-wall laws presented here can be used for such purposes.

In section 2.1 the analysis of the TBLE will be presented for two reasons. First we wish to strengthen the arguments and results from some of the previous authors. The analysis reported here clarifies how and under what circumstances previous results are applicable. Second, the modified analysis can be repeated for the separated case. This analysis is presented in section 2.2. The theoretical results for the separated case are derived from the same arguments as for the attached case. It is only the changed boundary condition at the wall that make the resulting expressions for the velocity profile different from the ones describing an attached boundary layer.

2.1. *The attached boundary layer*

The analysis of the TBLE will be divided into three parts. The first and second parts deal with the total shear stress in the inner region of the boundary layer, where the advective terms in the TBLE are neglected. The analysis in the first part will lead to a velocity profile in the viscous sub-layer, where also the Reynolds stress can be neglected. The overlap region is investigated in the second part.

The third part is devoted to the outer part of the boundary layer, where the viscous term in the TBLE is neglected. Together with the analysis of the

outer part, an integration of the TBLE with all terms included, gives some relations between mean flow parameters, such as shape factor and skin friction.

2.1.1. The inner region

The analysis of the inner region (near-wall flow) will be performed in more detail than the analysis of the outer part, since the low Reynolds number together with an adverse pressure gradient give a flow that differs substantially from the ZPG flow. Also, the results for the separated flow will be based on the analysis of the APG flow.

When neglecting the non-linear, advective terms in the equations describing the mean flow, the equation governing the inner part of the boundary layer is obtained. Using the inner length and velocity scales ν/u_τ and u_τ , the equation can be written,

$$0 = -\frac{\nu}{u_\tau^3} \frac{1}{\rho} \frac{dP}{dx} + \frac{d^2 u^+}{dy^{+2}} - \frac{d}{dy^+} \langle u'v' \rangle^+, \quad (3)$$

where $\langle u'v' \rangle$ is the Reynolds shear stress. If the term involving the pressure gradient is negligible small compared to the other terms, the equation reduces to the equation governing the inner part of a ZPG boundary layer. However, for strong APG cases at finite Reynolds numbers, this term cannot be neglected. Equation (3) can be integrated to give an expression for the total shear stress,

$$\tau^+ \equiv \frac{du^+}{dy^+} - \langle u'v' \rangle^+ = 1 + \frac{\nu}{u_\tau^3} \frac{1}{\rho} \frac{dP}{dx} y^+ \quad (4)$$

For a ZPG case, equation (4) predicts a constant shear stress of unity in the inner region.

The pressure gradient term in equation (4) is evidently important for the shear stress distribution in the inner part of the boundary layer. This was observed in, among others, the experiments by Bradshaw (1967), Samuel & Joubert (1974) and Skåre & Krogstad (1994), and the DNS by Spalart & Watmuff (1993) and Skote *et al.* (1998). It can be shown that the pressure gradient term decreases with increasing Reynolds number, and thus is important only for low Reynolds numbers. However, close to separation, where u_τ approaches zero, it is clear that the pressure gradient term becomes infinite, even for large Reynolds numbers.

When considering a strong APG or separation, the singularity mentioned above can be avoided by introducing the velocity scale u_p , defined in equation (2). To see this, we first formulate equation (4) as

$$\tau^+ = 1 + \left(\frac{u_p}{u_\tau} \right)^3 y^+. \quad (5)$$

The velocity scale u_p has to be used instead of u_τ if the last term in equation (5) becomes very large which happens if $u_\tau \ll u_p$, i.e. the boundary layer is close to separation. This was noted by Stratford (1959), Townsend (1961)

and Tennekes & Lumley (1972). By multiplying equation (5) by $(u_p/u_\tau)^2$, the following expression for $\tau^p \equiv \tau/(\rho u_p^2)$ as a function of $y^p \equiv y u_p/\nu$ is obtained,

$$\tau^p = y^p + \left(\frac{u_\tau}{u_p}\right)^2. \quad (6)$$

Equation (6) has the asymptotic form $\tau^p = y^p$ when separation is approached. Thus, in this rescaled form, the singularity is avoided.

There are three possible complications in the above analysis. First, the pressure gradient may depend on the normal coordinate. This was proved to be important when the analysis was compared with the data from the simulation of NM, see Skote & Henningson (1999). However, due to the straightforward boundary conditions used in the present simulation, no such dependence exists in the data presented here. The second complication is that the TBLE contains the streamwise derivative of longitudinal and normal Reynolds stresses. These terms may be important in a strong APG flow as was noted by Rotta (1962). A third complication is the non-linear inertia terms, which can influence the total shear stress as argued by McDonald (1969). However, in the present simulations these two terms are not important and will be disregarded in the following.

Now, in the viscous sub-layer the Reynolds shear stress approaches zero and equation (6) can be integrated to give,

$$u^p \equiv \frac{u}{u_p} = \frac{1}{2}(y^p)^2 + \left(\frac{u_\tau}{u_p}\right)^2 y^p. \quad (7)$$

In the limit of separation, when $u_\tau/u_p \rightarrow 0$, equation (7) reduces to

$$u^p = \frac{1}{2}(y^p)^2. \quad (8)$$

In viscous units, equation (7) becomes,

$$u^+ = y^+ + \frac{1}{2} \left(\frac{u_p}{u_\tau}\right)^3 (y^+)^2. \quad (9)$$

This equation reduces to the usual linear profile in ZPG case, when $u_p/u_\tau \rightarrow 0$.

The two expressions (5) and (6) are equivalent. It is in the limits of $u_\tau/u_p \rightarrow 0$ and $u_p/u_\tau \rightarrow 0$ respectively that the formulation becomes crucial. The same observation is true for the expressions (7) and (9). However, when plotting data from the rapidly varying separation bubble of NM, the scaling based on u_p gives a much better collapse of the profiles. In the scaling based on u_τ , the profiles are scattered, due to the strong variation of u_τ . In the simulations presented here, the pressure gradient is varying less violently.

2.1.2. *The overlap region*

The velocity profiles derived in this section will have asymptotic forms that are consistent with the profiles in the viscous sub-layer derived in the previous section. That is, the two velocity scales (u_τ and u_p), yield two different velocity

profiles, valid in the limits of ZPG ($u_p/u_\tau = 0$) and separation ($u_\tau/u_p = 0$) respectively. In flows between these asymptotic states (APG flows), the two scalings are equivalent and both give a velocity profile that depends on the Reynolds number and the pressure gradient through the ratio between u_τ and u_p .

We now proceed with the analysis by first considering the total shear stress. For the ZPG case, the scaling of the total shear stress with u_τ gives a self-similar profile ($\tau^+ = 1$). From equations (5) and (6) it is observed that neither u_τ nor u_p as velocity scale results in a self-similar expression. However, equation (4) can be formulated as

$$\tau^* \equiv \frac{1}{u_*^2} \left(\nu \frac{\partial u}{\partial y} - \langle u'v' \rangle \right) = 1, \quad (10)$$

where u_* is a velocity scale that depends on y and can be expressed in either viscous or pressure gradient units,

$$u_*^2 = u_\tau^2 + \frac{u_p^3}{u_\tau} y^+ = u_\tau^2 + u_p^2 y^p. \quad (11)$$

Thus, by scaling the total shear stress with u_* , a self-similar expression is obtained ($\tau^* = 1$). The velocity scale u_* reduces to u_τ if u_p becomes zero, i.e. for a ZPG boundary layer. If instead u_τ becomes zero, i.e. for a boundary layer at separation, the velocity scale becomes $u_* = u_p \sqrt{y^p}$. However, when $u_* = u_p \sqrt{y^p}$ is inserted in equation (10) we can write the equation as $\tau^p = y^p$, i.e. we use u_p as the velocity scale. Note that for the special case with $u_\tau = 0$, the velocity scale u_* is zero at the wall. This is natural since the velocity gradient is zero at the wall.

The logarithmic behavior of the turbulent boundary layer is obtained from the matching of the velocity gradient, or equivalently, the shear stress, in the inner and outer regions of the boundary layer. The matching also requires a consistency condition that results in the logarithmic friction law.

For the matching of the inner and outer equations, it is enough to observe that the total shear stress can be written in the form (10) in the inner part. In the outer part it is assumed that the velocity gradient can be written,

$$\frac{\partial u}{\partial y} = F' u_* / \Delta, \quad (12)$$

where F' is a function of a similarity variable (y/Δ) and Δ is the outer length scale. Equation (12) should be considered as the scaled formulation of the velocity gradient for the outer part, corresponding to the scaled velocity gradient for the inner part, which can be written as

$$\frac{\partial u}{\partial y} = f' u_*^2 / \nu, \quad (13)$$

where f' is a function of a similarity variable (yu_*/ν).

If the total shear stress is scaled with u_* in the outer and inner parts, and assumptions (12) and (13) are valid, then the matching of the total shear stress gives the equation,

$$y^* \left(\frac{\partial u}{\partial y} \right)^* = \frac{1}{\kappa}, \quad (14)$$

where a short notation is used for the scaled velocity derivative,

$$\left(\frac{\partial u}{\partial y} \right)^* \equiv \nu \frac{\partial u}{\partial y} \frac{1}{u_*^2}. \quad (15)$$

The scaled normal coordinate is

$$y^* \equiv y u_* / \nu = \sqrt{(y^+)^2 + (y^p)^3}. \quad (16)$$

For the ZPG case, for which $u_p = 0$, equation (14) is reduced to,

$$y^+ \frac{du^+}{dy^+} = \frac{1}{\kappa}. \quad (17)$$

When integrated, equation (17) gives the logarithmic velocity profile.

In the same way as equation (17) can be integrated to give the logarithmic law for the ZPG case, equation (14) above can be integrated to give a velocity profile in either viscous scaling ($u^+ \equiv u/u_\tau = f(y^+)$) or pressure scaling ($u^p \equiv u/u_p = g(y^p)$). Both of these expressions will depend on the ratio between u_τ and u_p , and are thus not self-similar. A self-similar profile of the form $u^* \equiv u/u_* = h(y^*)$ is not consistent with equation (10). This is further discussed at the end of this section.

If u_τ is chosen as velocity scale, the integration of equation (14) yields,

$$u^+ = \frac{1}{\kappa} \left(\ln y^+ - 2 \ln \frac{\sqrt{1 + \lambda y^+} + 1}{2} + 2(\sqrt{1 + \lambda y^+} - 1) \right) + B, \quad (18)$$

with

$$\lambda = \left(\frac{u_p}{u_\tau} \right)^3.$$

The expression (18) is not self-similar due to the term λ which is Reynolds number dependent. Equation (18) is the same expression as Afzal (1996) arrived at. It is also similar to the equation which Townsend (1961) derived from mixing length arguments.

If u_p is chosen as velocity scale, then (18) can be written,

$$u^p = \frac{1}{\kappa} \left(2\sqrt{\gamma^2 + y^p} + \gamma \ln y^p - 2\gamma \ln(\sqrt{\gamma^2 + y^p} + \gamma) \right) + C \quad (19)$$

where

$$\gamma = \frac{u_\tau}{u_p}.$$

For a ZPG boundary layer, for which $\lambda = 0$, equation (18) reduces to the logarithmic profile. In the other limit, at separation, when γ is zero, equation

(19) reduces to the half-power law,

$$u^p = \frac{1}{\kappa} 2\sqrt{y^p} + C, \quad (20)$$

which was first derived by Stratford (1959). Note that equation (20) can be rewritten in such a manner it is independent on the viscosity, as in the formulation by Stratford.

As mentioned earlier, it is not possible to solve equation (14) directly to obtain an expression for u^* as a function of only y^* . This is due to the scaled (with u_*) velocity gradient, which cannot be formulated independently of u_τ and u_p . The velocity gradient scaled with a constant velocity scale u_τ or u_p is, on the other hand, straightforward to express independently of the Reynolds number,

$$\nu \frac{\partial u}{\partial y} \frac{1}{u_\tau^2} = \left(\frac{\partial u}{\partial y} \right)^+ = \frac{du^+}{dy^+}. \quad (21)$$

Thus, in the ZPG case the equation permits a self-similar velocity profile (the logarithmic function). The same is true for the zero wall stress case (the half-power law). In all flows between these two asymptotic states, the velocity profile depends on the Reynolds number through the ratio between u_τ and u_p .

In other words, for all APG boundary layers, including the asymptotic states ZPG and separation, the total shear stress can be made self-similar by using the velocity scale u_* . For the ZPG and separating boundary layers, u_* reduces to a constant (y independent) velocity scale (u_τ and u_p respectively). This leads to that the velocity profile becomes self-similar for those two cases (due to equation (21) above). For all APG cases in between, the velocity scale u_* is not constant, and hence the velocity profile is not self-similar.

2.1.3. The outer part

The analysis of the integrated TBLE, together with the analysis of the outer part, where the viscous terms are neglected, was conducted thoroughly by Skote *et al.* (1998). Only the resulting equations, linking the mean flow parameters with each other, will be recapitulated.

The aim here is to simplify the equations under the assumption of self-similarity. The conditions for self-similarity and the resulting relations between mean flow parameters are presented. The reason for interest in self-similar flows originates from at least three arguments. First, the equation of motion are simpler to analyze. Second, turbulence models can be calibrated using a single profile, or investigated from an asymptotic approach. Third, calibration and determination of parameters such as friction velocity can be done in experiments.

If the viscous term is neglected in the equations describing the mean flow of a two-dimensional, incompressible, turbulent boundary layer, the equation governing the outer part of the layer is obtained. From this equation it is possible to deduce that a necessary condition for self-similarity is that a pressure

gradient parameter (denoted β) is constant,

$$\beta \equiv \frac{\delta^*}{\tau_w} \frac{dP}{dx} = \text{constant}. \quad (22)$$

Furthermore, if u_τ/U is regarded as constant and an outer length scale varies linearly, the condition $\beta = \text{constant}$ is fulfilled if the freestream variation is of the form $U \sim x^m$, which when specifying a profile becomes,

$$U = U_0 \left(1 - \frac{x}{x_0}\right)^m. \quad (23)$$

If this form of the freestream is inserted in the TBLE together with the assumption that the velocity defect and Reynolds shear stress, when scaled with the friction velocity, are functions of an outer variable η ,

$$\begin{aligned} (u - U)/u_\tau &= F(\eta), & -\langle u'v' \rangle / u_\tau^2 &= R(\eta), \\ \eta &= y/\Delta(x), & \Delta &= U\delta^*/u_\tau, \end{aligned} \quad (24)$$

the TBLE becomes,

$$\begin{aligned} & -2\beta F + \frac{\beta}{m}(1+m)\eta \frac{dF}{d\eta} \\ + \frac{u_\tau}{U} \left\{ -\beta F^2 + \frac{\beta}{m}(1+m) \frac{dF}{d\eta} \int_0^\eta F d\eta \right\} &= \frac{dR}{d\eta} + \frac{1}{Re_{\delta^*}} \frac{d^2 F}{d\eta^2}. \end{aligned} \quad (25)$$

The equation governing the outer part is obtained if the last term in equation (25) is neglected.

If F is of order unity, the terms within the bracket after u_τ/U can be neglected, which results in a linearization of the equation. This simplification is only valid in the limit of infinite Reynolds number, when $u_\tau/U \rightarrow 0$. However, closer to the wall, and for finite Reynolds number, F is of order U/u_τ and all terms in the equation are of the same order. Thus, when integrating from the wall to the freestream, the non-linear terms must be kept. The viscous term is also important since it is zero only for a boundary layer at the point of separation.

Thus, retaining all terms and integrating equation (25), the relationship,

$$m = -\frac{\beta}{H(1+\beta) + 2\beta}, \quad (26)$$

is obtained. H is the shape factor. The asymptotic result for infinite Reynolds number, when $u_\tau/U \rightarrow 0$, is obtained by setting H equal to unity.

In the present APG simulation the Reynolds stress profiles at different positions are not self-similar, due to the small variation of u_τ/U . For large Reynolds numbers, the profiles tend to a self-similar state. This can be seen from e.g. the experiments with a strong pressure gradient of Skåre & Krogstad (1994), or from calculations with turbulence models as in Henkes (1998) or Skote *et al.* (1998).

From the definition of β , equation (22), and the freestream profile used, equation (23), it follows that if m and the ratio u_τ/U are constants, then,

$$\Delta = \left(1 - \frac{x}{x_0}\right)\Delta_0. \quad (27)$$

All of these conditions and the resulting relations are investigated in the DNS data presented in section 3.2.1. Now the effect of a different velocity scale is investigated.

In the previous studies by Skote *et al.* (1998), the APG was not so strong that rescaling was required, neither in the inner nor in the outer region. For a strong APG or separated case, the scaling of the velocity defect with u_τ has to be reconsidered, following the arguments from the preceding sections.

As for the inner part, the rescaling merely means a change of the velocity scale from u_τ to u_p . When using u_p instead of u_τ as velocity scale, the parameter occurring in the TBLE is changed from β to β_p ,

$$\beta_p \equiv -\frac{\delta^*}{u_p^2}U\frac{dU}{dx} = \beta\left(\frac{u_\tau}{u_p}\right)^2 = \frac{\delta^*}{\nu}u_p. \quad (28)$$

The TBLE scaled with u_p is equation (25) multiplied by $(u_p/u_\tau)^3$, and integrated it gives the relation,

$$m = -\frac{\beta_p}{H\left(\left(\frac{u_\tau}{u_p}\right)^2 + \beta_p\right) + 2\beta_p}, \quad (29)$$

which is identical to relation (26). If $u_\tau \rightarrow 0$, the relation (29) reduces to,

$$m = -\frac{1}{H+2}, \quad (30)$$

which is also what (26) reduces to when $u_\tau \rightarrow 0$, i.e. when $\beta \rightarrow \infty$.

In the analysis of the TBLE with u_p instead of u_τ , the self-similar expressions (24) are replaced with the following expressions,

$$\begin{aligned} (u - U)/u_p &= F_p(\eta_p), & -\langle u'v' \rangle / u_p^2 &= R_p(\eta_p), \\ \eta_p &= y/\Delta_p(x), & \Delta_p &= U\delta^*/u_p. \end{aligned} \quad (31)$$

The scaling of the velocity defect with u_p cannot give self-similar profiles since β_p is not constant according to the definition (2) of u_p . The ratio u_p/U is not constant either. Thus, a theoretical expression for the outer part in a boundary layer close to separation must be based on another kind of scaling.

There have been many attempts to properly describe the velocity profile in the outer part of the boundary layer, both for ZPG and APG flows. Coles (1956) proposed a wake function for the description of the velocity profile. Since then a number of changes and refinements have been presented. Musker (1979), among others, proposed a velocity profile that is valid from the wall to the freestream, consisting of a logarithmic function and a wake function of the polynomial form. Dengel & Fernholz (1990) disregarded the form of the

original wake function, and propose a polynomial fit to the velocity profile. A different approach was chosen by Perry & Schofield (1973), who found their velocity scale by a fitting procedure similar to the Clauser plot in the ZPG case. They also related the velocity scale to the maximum shear stress, but no experimental data have confirmed this relation. Durbin & Belcher (1992) derived a three-layered structure of the turbulent boundary layer under a strong adverse pressure gradient. No experimental data have verified their scalings.

With this abundance of theories and proposed functions for the description of the velocity profile in the outer part, it is difficult to extract the 'best' theory, especially with those containing a large number of constants to be adjusted to obtain the best fit with DNS data. Therefore, in the present work, the velocity profile in the outer part will not be investigated with respect to the vast number of suggested profiles described above. We are content with a comparison between the velocity scales u_τ and u_p .

The difficulties in finding an appropriate description of the velocity profile in the outer part of the boundary layer in strong APG flows with or without separation, may be attributed to 'historical effects', i.e. the flow is not determined by local parameters (except for equilibrium layers), but is influenced by downstream and upstream conditions. This is consistent with the arguments of Perry (1966), who divided the boundary layer into a wall region, where the flow is determined by local parameters, and a 'historical region' where this local or 'regional similarity' does not apply.

2.2. *The separated boundary layer*

The TBLE cannot be used as a tool if a calculation of the downstream behavior of a separated boundary layer from given boundary condition is to be performed, Rotta (1962), Perry & Fairlie (1975). However, the TBLE can still be used for the analysis of local velocity profiles.

In this section the case of separation will be discussed. The limit of zero shear stress ($u_\tau/u_p \rightarrow 0$) was approached in the analysis above, and the asymptotic version of the expression for the velocity in the viscous sub-layer was equation (8), and in the logarithmic region it was equation (20). These two expressions were obtained by setting $u_\tau = 0$ in equation (7) and (19) respectively. Now, if a separated flow is considered, the definition of u_τ has to be reconsidered. In the separated region, $\frac{\partial u}{\partial y}$ is negative. Thus, the definition of u_τ in equation (1) involves a square root of a negative number. Instead, the definition will be changed so that the square root will be taken of a positive number. Thus, to proceed with the analysis of the equations, the definition of the friction velocity will have to be changed to

$$u_\tau \equiv \sqrt{-\nu \frac{\partial u}{\partial y} \Big|_{y=0}}. \quad (32)$$

This change will affect the analysis outlined in the previous section. It is the boundary condition at the wall used when integrating the TBLE that will

be different from the attached case. In this section the analysis will start with the inner part, continue with the overlap region, and end with the outer part.

The equation for the inner part (3) will not be changed since the scaling is not affected by the change of definition of u_τ . However, in the integration leading to equation (4), the boundary condition at the wall is used and will now, with the definition (32), change sign. Thus, the analysis is the same as in section 2.1. It is only the boundary condition that change the expression from equation (6) to

$$\tau^p = y^p - \left(\frac{u_\tau}{u_p}\right)^2. \quad (33)$$

For the velocity in the viscous sub-layer the expression becomes,

$$u^p = \frac{1}{2}(y^p)^2 - \left(\frac{u_\tau}{u_p}\right)^2 y^p, \quad (34)$$

instead of equation (7). Due to the changed boundary condition, the corresponding equation in viscous scaling, equation (9), will read as,

$$u^+ = -y^+ + \frac{1}{2}\left(\frac{u_p}{u_\tau}\right)^3 (y^+)^2. \quad (35)$$

Note that the equations (7) (attached boundary layer) and (34) (separated boundary layer) take the same form,

$$u^p = \frac{1}{2}(y^p)^2, \quad (36)$$

when $u_\tau/u_p \rightarrow 0$. This asymptotic form is equal for the two cases since the asymptotic state is the onset of separation. On the other hand, the corresponding equations in the viscous scaling, equations (9) and (35), have the asymptotic forms $u^+ = y^+$ and $u^+ = -y^+$ respectively. Thus, the assumption that viscous forces are stronger than the pressure gradient give different profiles in the attached and separated region.

From equations (7) or (35) it is possible to extract the maximum negative velocity and the position where it occurs. In pressure gradient scaling the maximum back-flow is $-\frac{1}{2}\left(\frac{u_\tau}{u_p}\right)^4$ at $y^p = \left(\frac{u_\tau}{u_p}\right)^2$. These results are valid if the back-flow maximum is located in the viscous sub-layer.

Now the logarithmic part of the boundary layer will be discussed. According to equation (33), the velocity scale that produce a self-similar shear stress ($\tau^* = 1$) is,

$$u_*^2 = -u_\tau^2 + \frac{u_p^3}{u_\tau} y^+ = -u_\tau^2 + u_p^2 y^p. \quad (37)$$

By inserting either form of u_* into equation (14), two different expressions for the velocity profile are obtained. Using the viscous scaling yields,

$$u^+ = \frac{1}{\kappa} \left[2\sqrt{\lambda y^+ - 1} - 2 \arctan \left(\sqrt{\lambda y^+ - 1} \right) \right] + B, \quad (38)$$

with

$$\lambda = \left(\frac{u_p}{u_\tau} \right)^3.$$

By using the pressure gradient scaling we obtain,

$$u^p = \frac{1}{\kappa} \left[2\sqrt{y^p - \gamma^2} - 2\gamma \arctan \left(\sqrt{\frac{y^p}{\gamma^2} - 1} \right) \right] + C, \quad (39)$$

where

$$\gamma = \frac{u_\tau}{u_p}.$$

The logarithmic dependence has been replaced by the arctan function. However, the asymptotic function (20) is recovered from equation (39) when $u_\tau/u_p \rightarrow 0$.

The equation (38) was actually derived by McDonald (1969) from Townsend's extended log law, however with the velocity scale u_p replaced with the shear stress gradient. McDonald argues that the shear stress gradient is different from the streamwise pressure gradient, and that the deviation originates from inertia effects.

After the analysis of the inner and logarithmic parts, we now proceed with the outer part. Since the separation (at least the weak one considered here) is a phenomenon confined to the inner part of the boundary layer, the outer part is not affected. However, the integration of the TBLE, presented in section 2.1.3, are affected since the boundary condition will change for a separated boundary layer compared to the attached one.

When integrating equation (25) in pressure gradient scaling, the changed boundary condition results in the relation,

$$m = - \frac{\beta_p}{H \left(- \left(\frac{u_\tau}{u_p} \right)^2 + \beta_p \right) + 2\beta_p}, \quad (40)$$

This relation is almost identical with the relation (29), and the only difference is the sign in front of u_τ^2 , which enters through the boundary condition at the wall. The asymptotic version for vanishing wall shear stress is the same, equation (30).

3. Direct numerical simulations

The numerical code and a discussion about the resolution required are presented in section 3.1. The results from the simulations will be presented in two sections. The general description of the flow is presented in section 3.2. In section 3.3 the mean flow will be presented and compared to the theoretical results from section 2.

3.1. Numerical considerations

The code used for simulation is only a tool to provide the data wanted. However, the complexity of numerical issues makes it interesting to present the basic ideas behind the numerical solution procedure. Especially in combination with the use of super computers, the computational algorithm can itself lead to research in its own right.

3.1.1. Numerical method and parallelization

The code used for the direct numerical simulations (DNS) was developed at KTH and FFA, Lundbladh *et al.* (1999). The numerical approximation consists of spectral methods with Fourier discretization in the horizontal directions and Chebyshev discretization in the normal direction. Since the boundary layer is developing in the downstream direction, it is necessary to use non-periodic boundary conditions in the streamwise direction. This is possible while retaining the Fourier discretization if a fringe region is added downstream of the physical domain. In the fringe region the flow is forced from the outflow of the physical domain to the inflow. In this way the physical domain and the fringe region together satisfy periodic boundary conditions. The fringe region is implemented by the addition of a volume force F , to the Navier-Stokes equations:

$$\frac{\partial u_i}{\partial t} + u_j \frac{\partial u_i}{\partial x_j} = -\frac{1}{\rho} \frac{\partial p}{\partial x_i} + \nu \frac{\partial^2 u_i}{\partial x_j^2} + F_i. \quad (41)$$

The force

$$F_i = \lambda(x)(\tilde{u}_i - u_i) \quad (42)$$

is non-zero only in the fringe region; \tilde{u}_i is the laminar inflow velocity profile which the solution u_i is forced to and $\lambda(x)$ is the strength of the forcing. The form of $\lambda(x)$ is designed to minimize the upstream influence. For an analysis of the fringe region technique, the reader is referred to Nordström *et al.* (1999).

Time integration is performed using a third order Runge-Kutta method for the advective and forcing terms and a Crank-Nicolson method for the viscous terms. A 2/3-dealizing rule is used in the streamwise and spanwise direction.

The numerical code is written in FORTRAN and consists of two major parts, one linear part where the equations are solved in spectral space, and one non-linear part where the non-linear terms in the equations are computed in physical space. The linear part needs data for one spanwise (z) position at a time since the equations are solved in the wall normal (y) direction. The non-linear part needs data for one y position at a time since the FFT is performed in the horizontal directions (spanwise and streamwise). The flow variables are stored at an intermediate level with spectral representation in the horizontal directions and physical representation in the y direction. All spatial derivatives are calculated with spectral accuracy. The main computational effort in these two parts is in the FFT.

The simulations were performed to a large extent on computers with distributed memory. The parallelization and optimization of the code for these type of computers were performed by Alvelius & Skote (2000). Communication between processors is necessary when the different operations on the data set are to be performed in the two different parts of the code. The data set (velocity field) is divided between the different processors along the z direction. Thus, in the linear part, no communication is needed. When the non-linear terms are calculated, each processor needs data for a horizontal plane. The main storage is kept at its original position on the different processors. In the non-linear part each processor collects the two-dimensional data from the other processors, on which it performs the computations and then redistributes it back to the main storage.

The boundary conditions are no-slip at the wall and at the freestream the normal derivative of the streamwise and spanwise velocity components are set to zero, while for the normal component the prescribed value of the APG is used,

$$\frac{\partial v}{\partial y} = \frac{\partial V_{APG}}{\partial y} = -\frac{\partial U_{APG}}{\partial x}. \quad (43)$$

These boundary conditions ensures that the prescribed APG is obtained.

3.1.2. Numerical parameters

The simulations were performed on various computers. The tuning of the pressure gradient for the desired flow situation was performed on a Cray T3E at NSC in Linköping, using 32 processors. After the design of the pressure gradient, a simulation with 20 million modes was performed on an IBM SP2 at PDC, KTH in Stockholm, using 32 processors. The results presented here are mainly from a second simulation with 40 million modes performed at the National Aerospace Laboratory (NAL), Tokyo. The same (with some differences due to the different types of processors) code was used on all three computers, using MPI (Message-Passing Interface) for the communication between the processors. The numerical method and the simulation performed at NAL was presented at the Parallel CFD 2000 conference in Trondheim.

The computer used at NAL was the Numerical Wind Tunnel (NWT), a parallel computer that consists of 166 vector processors from Fujitsu. The maximum performance on each processor is 1.7 Gflop/s. The main difference from the other two computers (CRAY T3E and IBM SP2) is the type of processor. While the other two consist of super-scalar processors, the NWT utilizes vector processors. These processors give a higher performance for each of the processing elements. The fast Fourier transforms (FFT), for which most of the time is spent during the simulation, have different structure for the scalar and vector processors.

The simulations start with a laminar boundary layer at the inflow which is triggered to transition by a random volume force near the wall. All the

quantities are non-dimensionalized by the freestream velocity (U) and the displacement thickness (δ^*) at the starting position of the simulation ($x = 0$), where the flow is laminar. At that position $Re_{\delta^*} = U\delta^*/\nu = 400$. The length (including the fringe), height and width of the computation box were $700 \times 65 \times 80$ in these units. The fringe region has a length of 100 and the trip is located at $x = 10$.

Results from two simulations are presented. One, which is called APG1, is a boundary layer subject to a strong APG. The flow in APG1 is everywhere attached. The second, which is called SEP, is a boundary layer under even stronger APG, and the flow is separated for a large portion.

Two different resolutions were used for the simulations. For APG1 the number of modes was $512 \times 193 \times 192$. After a simulation of SEP with the same resolution, a larger simulation was performed using the NWT. The number of modes in this simulation was $720 \times 217 \times 256$, which gives a total of 40 million modes or 90 million collocation points.

The simulations were run for a total of 7500 time units (δ^*/U), and the sampling for the turbulent statistics was performed during the last 2500 time units. The statistics were collected during the simulations and averaged in the spanwise direction. No filtering of the statistics has been used.

3.1.3. Resolution check

The simulation of a separated boundary layer was performed with two different resolutions and could be compared with each other. The turbulent statistics for both resolutions were computed from the same amount of simulation time. The general behavior in the streamwise direction is the same for the two resolution, i.e. there are no large differences in parameters such as friction velocity, shape factor etc. There were some differences in the region where the back-flow has its largest magnitude, which is now further investigated. Velocity profiles from two downstream positions are shown in figure 1, one at $x = 350$ where the back-flow is strongest, and one at $x = 500$, where the boundary layer is attached. A large part of the profile from the less resolved simulation at the point of maximum back-flow ($x = 350$) is below the profile from the well resolved simulation. However, close to the wall they collapse. In the attached region, the two profiles are essentially similar. Thus, the region where strong back-flow occurs is sensitive to the resolution, which means that caution is needed when simulating this type of flow. Also in the Reynolds shear stress some differences could be detected, most notably in the outer region, near the freestream. In the attached region there were no differences between the two resolutions for the Reynolds stresses. It should be noted that even though the history effects can influence the boundary layer downstream of reattachment, (see e.g. the investigations of Alving & Fernholz (1996)), the differences upstream of reattachment in the the two resolutions do not influence the boundary layer in the attached region.

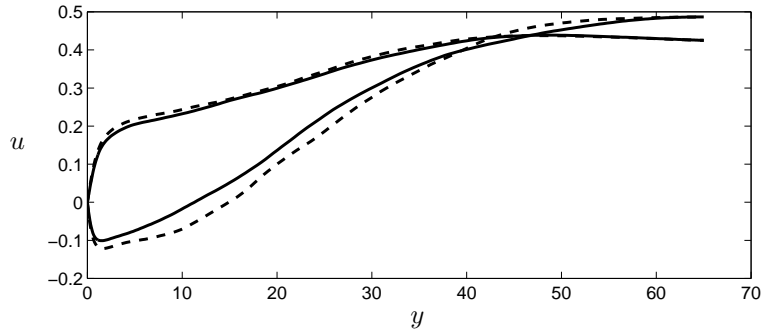


FIGURE 1. SEP: Velocity profile in the separated region at $x = 350$ and in the attached region at $x = 500$. — $720 \times 217 \times 256$ modes; - - $512 \times 193 \times 192$ modes.

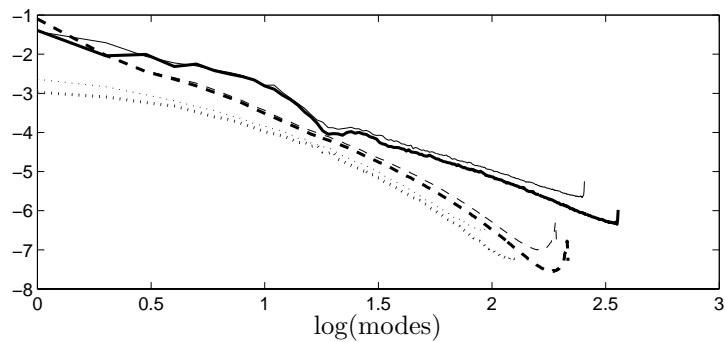


FIGURE 2. SEP: Energy contained in modes in — x ; - - y ; \cdots z . Thick lines: $720 \times 217 \times 256$; Thin lines: $512 \times 193 \times 192$.

This investigation shows that the lower resolution is sufficient for the attached region, while in the separated region, the high resolution is crucial for capturing the correct behavior.

Comparison with the resolution in the simulations by NM and SC is possible by rescaling the size of the box of their simulations in the coordinates of the present simulation and divide with number of collocation points. The result is shown in table 1. The resolution is better for the present simulation than in NM in all three directions, even though their method has second order accuracy while our method, as in SC, is spectral.

To further confirm the resolution we show the energy in the flow as function of the spectral modes for the two resolutions in figure 2. The thick lines are from the well resolved case. Note that the two velocity fields are from different times, thus the curves from the two cases do not collapse. The energy decays consistently in the three directions when the resolution is refined. The small

	present	NM	SC
Δx	0.65	0.85	0.57
Δy	0.30	0.41	0.27
Δz	0.21	0.48	0.21

TABLE 1. Comparison of resolution between the present simulation and the simulations by SC and NM.

contamination in the highest modes moves to higher wavenumbers as resolution is increased.

3.2. General description of the flow

The general behavior of the mean flow parameters is described and discussed in section 3.2.1. The instantaneous velocity field will be presented in section 3.2.2, where a qualitative description of the structures appearing in the flow will be afforded. In section 3.2.3 a general description of some turbulence statistics are presented.

3.2.1. Mean flow parameters

In earlier simulations of APG turbulent boundary layers by the authors of the present work, Skote *et al.* (1998), the freestream velocity varied according to a power law in the downstream coordinate, $U \sim x^m$. The motivation for this was that a self-similar profile in the outer part could be developed. In the simulations presented here, the aim was to get a boundary layer as close to a separated state as possible. The tuning of the pressure gradient is extremely time consuming since the boundary layer has a slow response to any change in the pressure distribution.

The pressure gradient is determined through the freestream velocity, which is of the same functional form as in Skote *et al.* (1998),

$$U = \left(1 - \frac{x}{x_0}\right)^m. \quad (44)$$

The two parameters that can be changed are x_0 and m , and they are summarized in table 2.

The freestream velocity (U) for the two simulations, APG1 and SEP, are shown in figure 3, together with the skin friction (C_f). As seen from the figure, a small change in the freestream velocity has a great impact on the skin friction. A number of simulations were performed to obtain a boundary layer with a wall shear stress as close to zero as possible. These two simulations are the ones where we obtained u_τ closest to zero, and were therefore continued for a long time to get good statistics. The resolution was discussed in section 3.1, and the conclusion was that both simulations can be considered well resolved.

Even if the boundary condition (U) is almost the same for the two simulations, the resulting boundary layers contain very different flows. In APG1

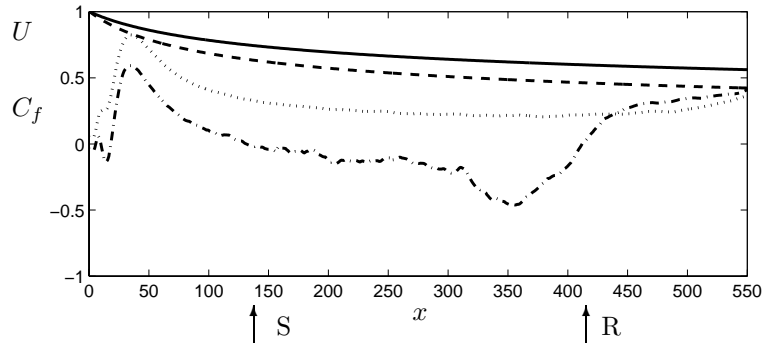


FIGURE 3. APG1: — U ; \cdots $C_f \times 100$. SEP: - - U ; - · - $C_f \times 100$. S and R denotes point of separation and reattachment respectively for SEP.

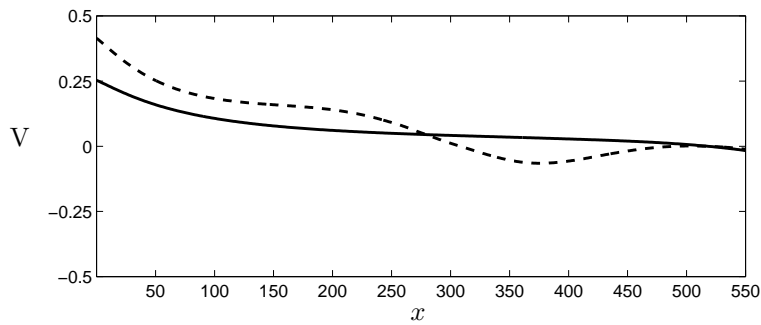
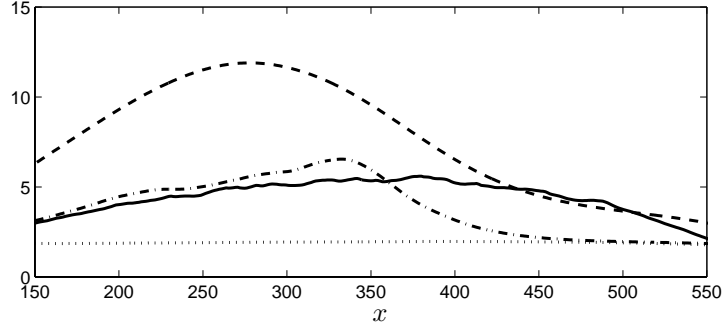
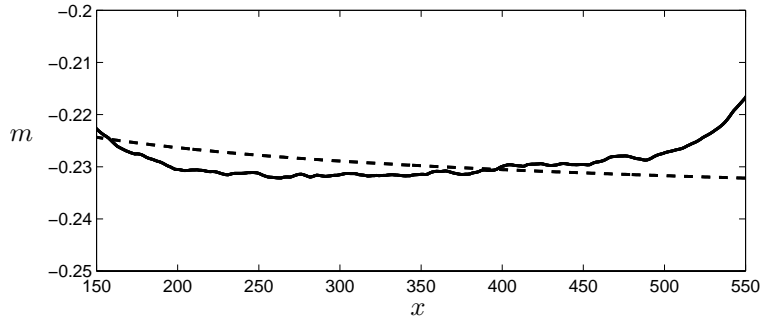


FIGURE 4. APG1: — V . SEP: - - V .

the boundary layer is subject to a strong APG, but is everywhere attached. In SEP the boundary layer is separated for a large portion of the computational domain. The resulting normal velocity at the freestream boundary (V) is shown for the two cases in figure 4.

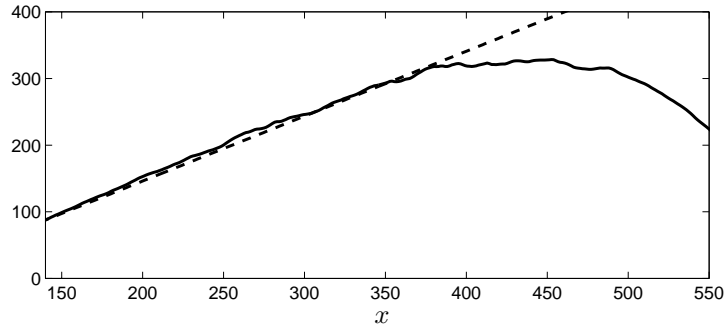
The parameter β for APG1 is shown in figure 5, and is approximately constant. The shape factor from APG1 is almost exactly constant over the whole domain $x = 150 - 550$. The corresponding parameter β_p from SEP is also shown in figure 5 together with the shape factor. The boundary layer with separation is evidently not near equilibrium since β_p is not constant. The shape factor also varies strongly downstream as a consequence of the non-equilibrium as seen in figure 5.

Since β is constant in the APG1 case, it is possible to check the relation given by equation (26). Using β and H from APG1 (shown in figure 5), equation (26) yields an m close to -0.23 , shown as the solid line in figure 6. However, the value of m was set to -0.25 in the simulation. The difference in the value of m is explained by the non-uniqueness of the two parameters in the freestream

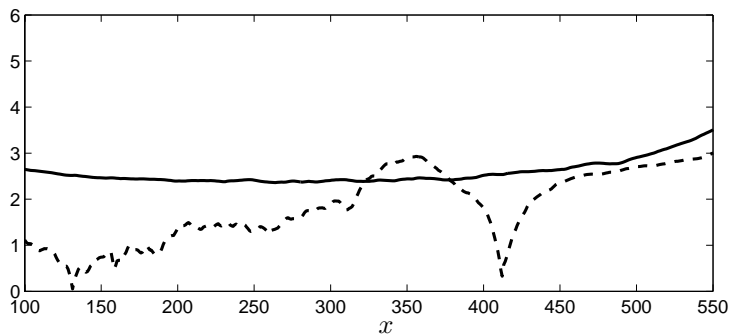
FIGURE 5. APG1: — β ; \cdots H . SEP: -- $\beta_p/10$; - · - H .FIGURE 6. APG1: — m from equation (26); - - m from equation (44) with $x_0 = -50$.

velocity distribution. A specific distribution of U can be closely represented by different values of m and x_0 . Thus, the imposed distribution of U can be obtained by applying a different set of the parameters m and x_0 than used in the definition of the distribution. However, the value of x_0 in the simulation can be determined by looking at the resulting outer length scale, Δ , shown in figure 7. The dashed line is equation (27) with $x_0 = -50$, thus a different value than the one used in the profile for U , which is $x_0 = -62$. By using the value of $x_0 = -50$, the exponent m can be calculated from the expression (44). The resulting m is shown as the dashed line in figure 6, matching approximately the m from equation (26). Thus, even if the freestream velocity is defined with the parameters $x_0 = -62$ and $m = -0.25$, the same freestream distribution is represented by $x_0 = -50$ (taken from the distribution of Δ) and $m \approx -0.23$ (the exact value of m is the dashed line in figure 6). These latter values of m and x_0 are the apparent parameters actually felt by the boundary layer and are called m^a and x_0^a in table 2.

The ratio between the two velocity scales (u_τ/u_p) is shown in figure 8 for the two cases. The ratio is fairly constant for APG1, and even in the case of separation the variation is not violent. This is in strong contrast to the rapid

FIGURE 7. APG1: — Δ ; - - equation (27) with $x_0 = -50$.

Case	m	x_0	m^a	x_0^a
APG1	-0.25	-62	-0.23	50
SEP	-0.35	-50		

TABLE 2. Freestream parameters. m and x_0 are the values in the simulation specifying the freestream velocity through equation (44). x_0^a and m^a are the actual values corresponding to equilibrium theory.FIGURE 8. u_τ/u_p . APG1: — ; SEP: - -.

separation and attachment simulated by SC and NM. The constant ratio will have some consequences for the scaling of the velocity profiles shown in section 3.3.

The strong decrease in the skin friction before the reattachment cannot be explained by the mean momentum equation alone. The point of reattachment cannot be predicted either, but can be detected from the behavior of the normal velocity at the freestream boundary (figure 4). In the beginning of the computational domain the flow out of the box is generated by the strong decrease in the streamwise velocity. Later, the flow is inward, due to the fringe

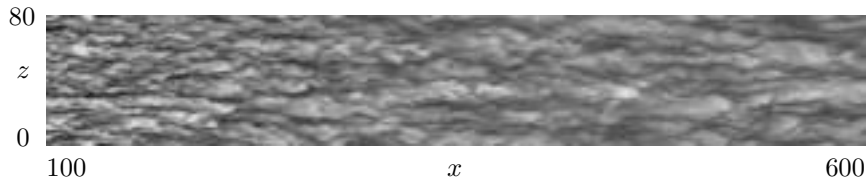


FIGURE 9. APG1: Streamwise velocity fluctuation in a plane at $y^+ = 10$. The dark area represents low-speed fluid

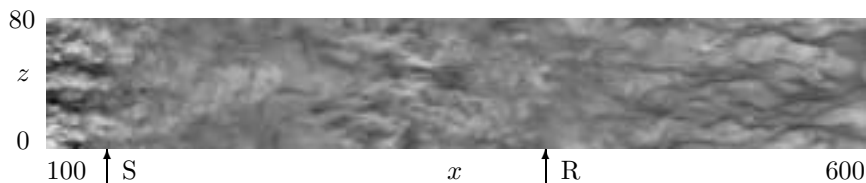


FIGURE 10. SEP: Streamwise velocity fluctuation in a plane at $y^+ = 10$. The dark area represents low-speed fluid

region, where the original, laminar boundary layer is restored. With a longer computational box, the point of reattachment would move downstream. The influence of the fringe is however not unphysical, since it only determines the boundary condition at the outflow. The boundary layer has to end somewhere, and this scenario is just one example. If a ZPG or APG layer is studied, where the exact form of the pressure gradient is important, the upstream influence of the fringe is important, since the equilibrium conditions are changed.

3.2.2. Structures in the flow

The streamwise velocity fluctuations form elongated structures near the wall in a ZPG boundary layer. It is generally thought that the structures are weakened in an APG flow. This is illustrated in figure 9, where shades of positive and negative fluctuations are shown for the APG1 case. The figure shows the whole computational box in the spanwise direction but the transitional part and fringe region are excluded in the streamwise direction. The normal position is $y^+ = 11.8$ in the beginning and $y^+ = 9.2$ at the end. The length in the streamwise direction is about 3400 in viscous units based on u_τ at $x = 350$. The structures are weakened at the end of the domain as compared with those in the beginning, showing the damping effect of the APG on the structures. The spacing between the structures increases from 100 (the same as for a ZPG layer) at the beginning to about 130 at the end, based on the local u_τ .

The SEP case is shown in figure 10. The normal position is also in this case around $y^+ = 10$ and the length of the region shown is about 2400. There are still some structures in the separated flow, though not at all as long and frequent as in APG1. Before separation, which occurs at approximately $x = 140$, the streaks are visible, but are rapidly vanishing in the beginning of the separated

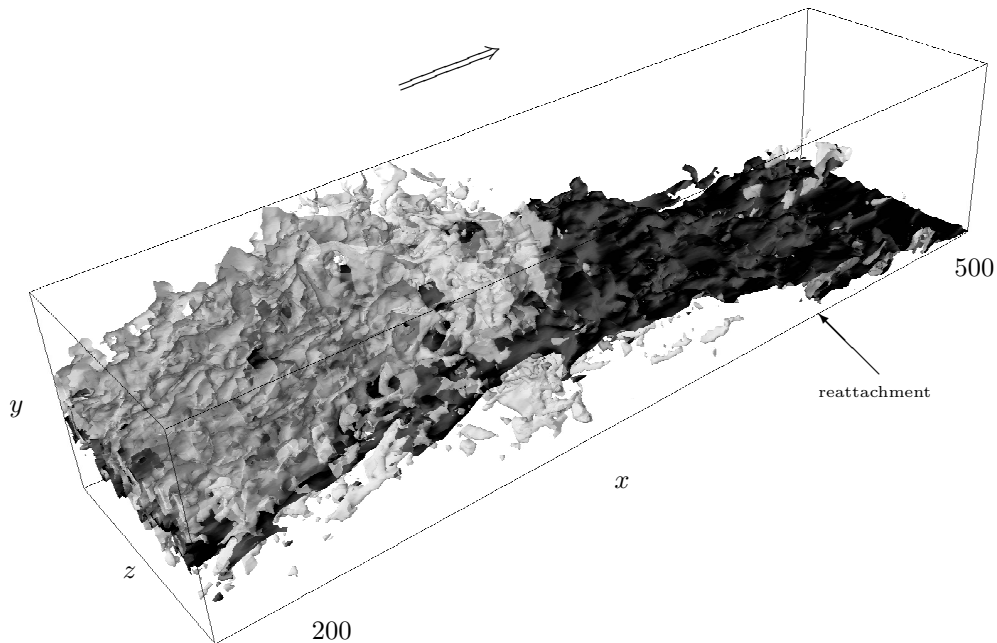


FIGURE 11. The separated boundary layer. Only a part of the computational box is shown. The light grey structures represent positive normal velocity and the darker ones represent positive streamwise velocity.

region. There is notable increase in the streak formation around $x = 350$, where the friction coefficient is at its lowest values, c.f. figure 3. Thus, there are indications that streaks may reappear in a separated region if the back-flow is strong enough. After the reattachment at $x = 412$ the streaks are not immediately appearing, but are clearly visible after $x = 450$.

To illustrate some more features of the instantaneous flow structures in the separated case, contour plots of constant streamwise and normal velocity are plotted in a part of the computational box. In figures 11 and 12, the streamwise velocity, plotted in dark grey color, show a less ordered structure than in a ZPG boundary layer. However, the constant streamwise velocity show the same features above the separation bubble as after the reattachment point. The sheet formed by the constant value is bent upward over the recirculation region and comes down again when approaching reattachment. This is in agreement with various experimental observations, see the introduction. In figure 11, a positive constant value of the normal velocity is shown in light grey color. The

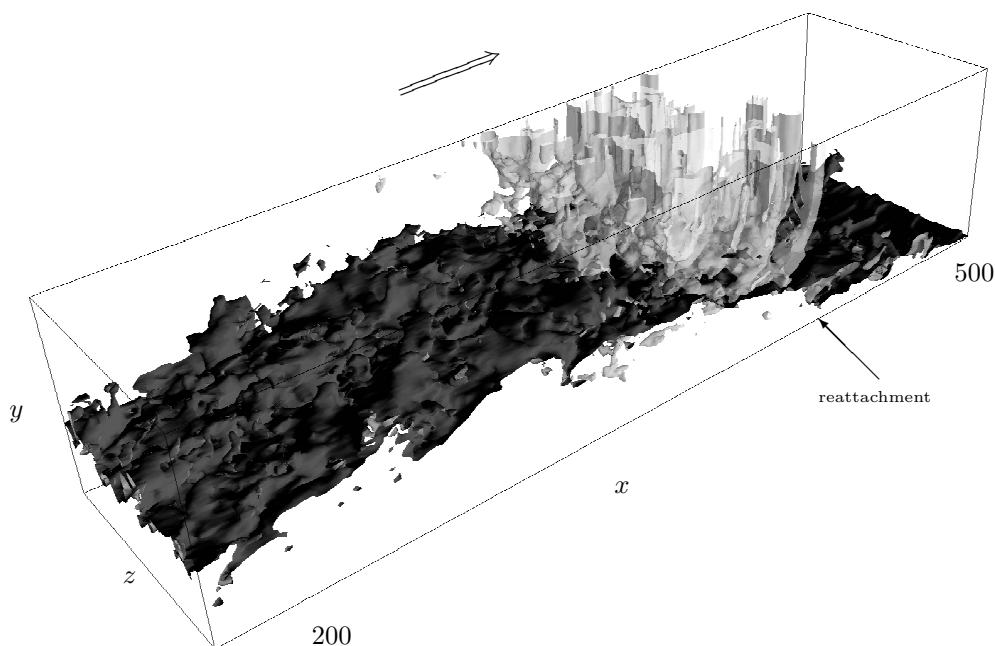


FIGURE 12. The separated boundary layer. Only a part of the computational box is shown. The light grey structures represent negative normal velocity and the darker ones represent positive streamwise velocity.

normal velocity is of the same disorganized form as the streamwise velocity. An opposite effect is revealed in figure 12, where a negative value of the normal velocity is shown. Here the structure is more ordered and forms tube-like structures where the fluid rushes from the freestream down towards the wall.

3.2.3. Turbulence statistics

A general description of the turbulent kinetic energy and its production is presented here. In this section the scaling of the turbulent statistics is based on the local freestream velocity. For the APG1 case the development of the turbulent kinetic energy is typical for an APG turbulent boundary layer. In figure 13 contours of constant levels of turbulent kinetic energy from 0.0005 to 0.006 are shown. The peak value is at all streamwise positions around 0.006. It is slightly larger in the beginning and decreases slowly downstream, while the position for the peak is shifted outward from $y = 4$ at $x = 150$ to $y = 18$ at $x = 550$. The turbulent kinetic energy development in SEP is more complicated

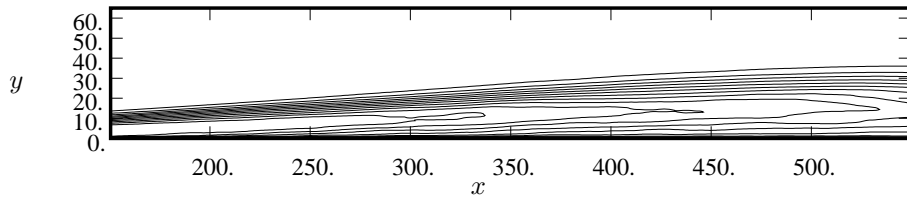


FIGURE 13. APG1: contours of turbulent kinetic energy.

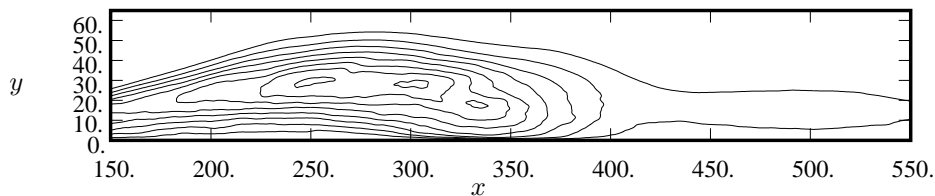


FIGURE 14. SEP: contours of turbulent kinetic energy.

and the discussion will be made with the aid of figure 14. In figure 14 contours of constant levels of turbulent kinetic energy from 0.005 to 0.025 are shown. At $x = 150$ the boundary layer has barely separated and the energy has one maximum of 0.0016 located far out in the boundary layer (approximately at $y = 18$). Further downstream, at position $x = 250$, the energy maximum has shifted outward to $y = 30$ with the larger value 0.025. The profile then stays approximately the same until the maximum starts to decrease and is moving towards the wall after $x = 330$. When comparing with the mean streamwise velocity in figure 15, it is noted that the peak in turbulent kinetic energy is located outside the recirculation zone. This was also noted by SC and Alving & Fernholz (1996) among others, (see the introduction in the present work). At $x = 350$ the profile of the energy is almost identical with the one at $x = 150$, but the maximum continues to decrease downstream, even though the location ($y = 18$) of the maximum is constant. The boundary layer is still subjected to an adverse pressure gradient, and the peak located far out in the boundary layer is a consequence of this. Nothing spectacular happens at the point of reattachment ($x = 412$). The peak value is stabilized after $x = 450$ at a value of 0.006, which is the same value as observed in the APG1 case.

The shear stress contribution to the production is shown in figure 16 for SEP. Approximately the same behavior as for the energy itself is observed up to $x = 330$. The maximum occurs closer to the wall, but still above the recirculation region. The streamwise Reynolds stresses do contribute to the production (not shown in the figure), but their contribution is fluctuating rapidly over the boundary layer and is much smaller than the production originating from

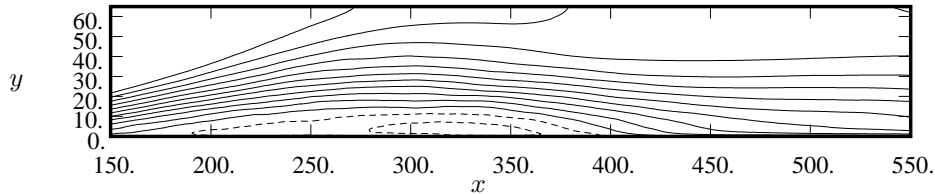


FIGURE 15. SEP: contours of mean velocity. Positive values shown as solid lines, negative as dashed.

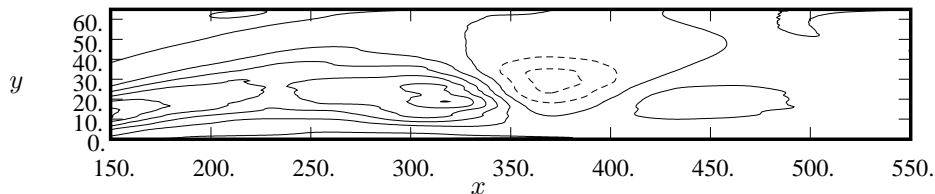


FIGURE 16. SEP: contours of production of turbulent kinetic energy. Positive values shown as solid lines, negative as dashed.

the shear stress, except close to the wall at some streamwise positions. From figure 16 it is also observed that there is a negative production (destruction) of turbulence kinetic energy in an area away from the wall, upstream of reattachment. This was also observed in the DNS of SC. The destruction is not a contribution from the streamwise production, but originates from positive values of the Reynolds shear stress in that region. In the DNS of NM no negative total production in the middle of the layer occurred, even if the production of Reynolds shear stress showed negative values both close to the wall and in the middle of the boundary layer. The destruction, and hence the positive values of the Reynolds shear stress, occur in the same region of the flow where the tube-like structures in the downward normal velocity are visible, c.f. figure 12.

3.3. Comparison with analysis

To compare the DNS data with the results from section 2, the mean flow profiles will be presented in different scalings and from different parts of the boundary layer. From figure 1 it is observed that the back-flow is very weak compared to the freestream velocity. The portion of the boundary layer where back-flow exists is small compared to the portion of positive streamwise velocity. But, the flow close to the wall is of course important, because it determines many of the features of the flow that are crucial from an engineering aspect.

From APG1 the data is compared with the results from the analysis of the TBLE for an attached boundary layer (section 2.1). From SEP the data

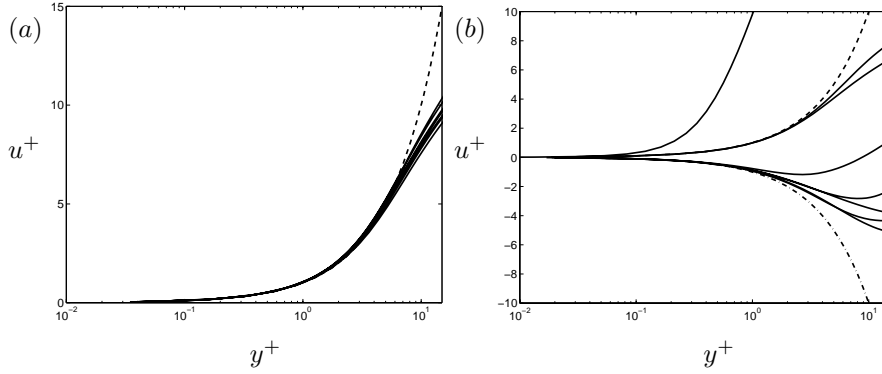


FIGURE 17. Velocity profiles at $x = 150$ to $x = 500$. a) APG1: — DNS; - - $u^+ = y^+$. b) SEP: — DNS; - - $u^+ = y^+$; - · - $u^+ = -y^+$.

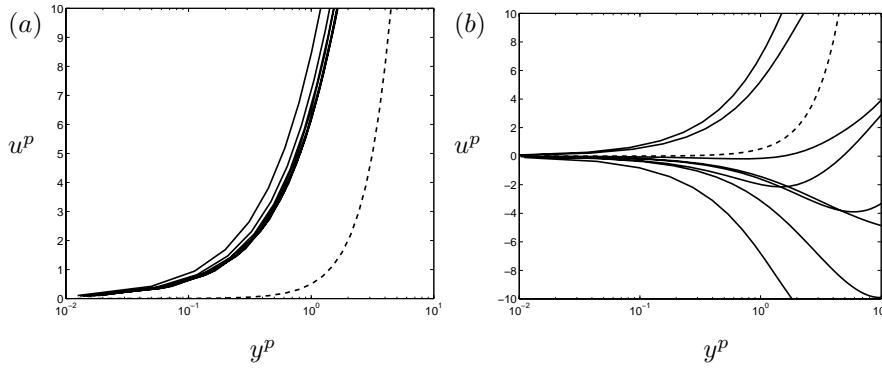


FIGURE 18. Velocity profiles at $x = 150$ to $x = 500$. a) APG1: — DNS; - - $u^p = \frac{1}{2}(y^p)^2$. b) SEP: — DNS; - - $u^p = \frac{1}{2}(y^p)^2$.

is compared with the results from the analysis of the TBLE for a separated boundary layer (section 2.2).

3.3.1. The viscous sub-layer

The near-wall profiles are plotted in the viscous scaling in figure 17 and are compared with the profiles given by the asymptotic versions of equations (9) and (35). For APG1 the collapse is good as seen in figure 17a. For the case SEP, shown in figure 17b, the profiles close to the $u^+ = y^+$ profile are the two in the attached region at positions $x = 450$ and $x = 500$. The profiles furthest from both asymptotes is from the positions closest to separation and reattachment, while the lowest (closest to $u^+ = -y^+$) is from the position with strongest back-flow.

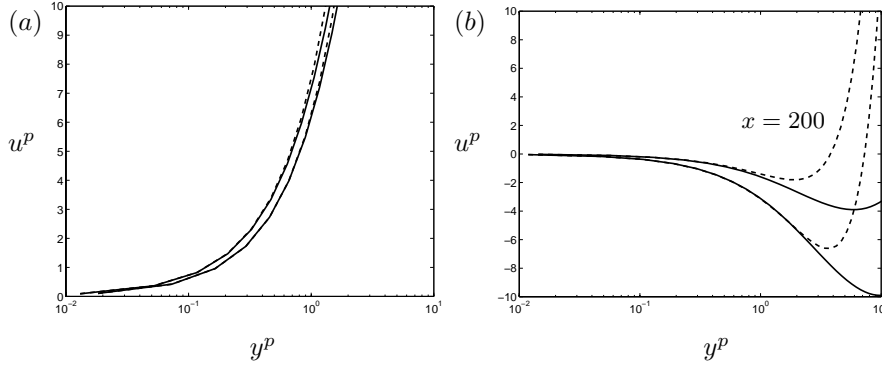


FIGURE 19. Velocity profiles in pressure gradient scaling. a) APG1: — DNS; - - $\frac{1}{2}(y^p)^2 + (\frac{u_\tau}{u_p})^2 y^p$. b) SEP: — DNS; - - $\frac{1}{2}(y^p)^2 - (\frac{u_\tau}{u_p})^2 y^p$.

In figure 18 the same profiles are shown in pressure gradient scaling and are compared with the profiles given by the asymptotic expression (36), which is the same for the attached and separated case. The spreading is the same as in the viscous scaling. That the profiles spread equally in the viscous scaling as in the pressure gradient scaling is due to the fact that the ratio u_τ/u_p is nearly constant, see figure 8. This is in strong contrast to the simulation of NM, where the variation in u_τ was enhanced by the rapidly growing pressure gradient. In their simulation, the velocity profiles collapsed much better when scaled with u_p than u_τ , (see Skote & Henningson (1999)). Figure 18 shows that the profiles are further from the asymptotic state (separation), than in the viscous scaling (figure 17), where the profiles showed some similarity with the asymptotic (ZPG) profile.

Velocity profiles in the pressure gradient scaling at two downstream positions are shown in figure 19, together with the theoretical expressions for the velocity profile in the viscous sub-layer. For APG1 (figure 19a) the positions are $x = 200$ and $x = 450$, and for SEP (figure 19b) they are $x = 200$ and $x = 300$. Here the asymptotic curve is not shown, but the pressure gradient dependent curves from equation (34) are shown. The DNS profiles and the corresponding curves given by equation (34) follow each other and show that even if the profiles are far from the asymptotic state (as shown in figure 18), the inclusion of the pressure gradient term gives a good agreement.

In summary, figure 17 shows that the scaling with u_τ works for APG1 but not for SEP. Figure 18 shows that the scaling with u_p does not work for APG1, nor for SEP, while figure 19 shows that with the inclusion of the pressure gradient term, the scaling with u_p works well in both cases.

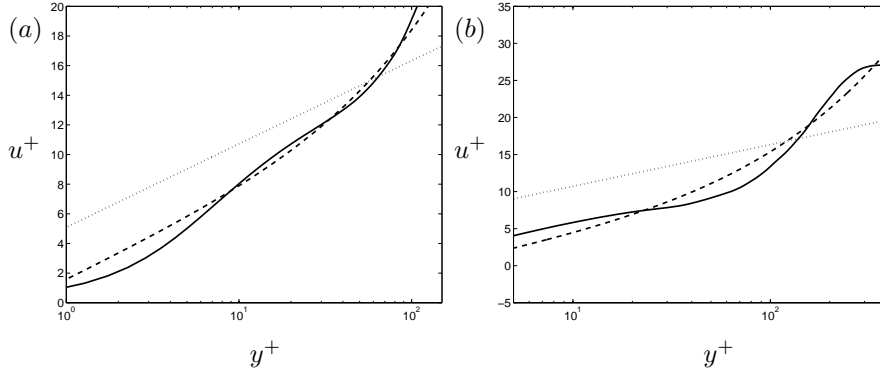


FIGURE 20. a) APG1: Velocity profile at $x = 350$. — DNS; - - equation (18) with $\kappa = 0.41$ and $B = 1.5$; $\cdots u^+ = \frac{1}{0.41} \ln y^+ + 5.1$. b) SEP: Velocity profile at $x = 450$. — DNS; - - equation (18) with $\kappa = 0.41$ and $B = -2$; $\cdots u^+ = \frac{1}{0.41} \ln y^+ + 5.1$.

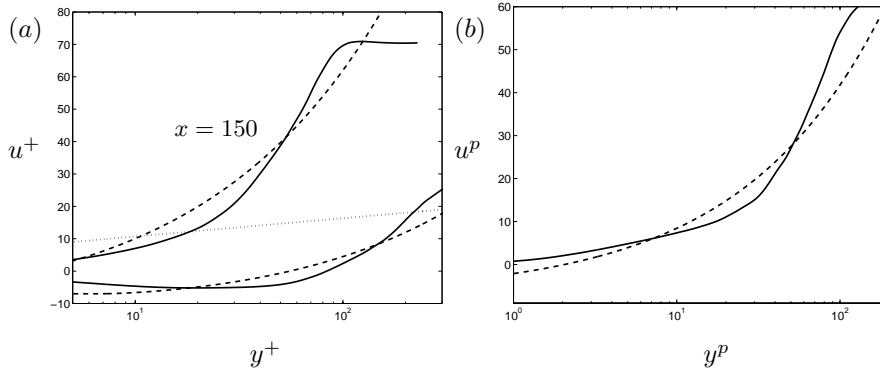


FIGURE 21. a) SEP: Velocity profiles at $x = 150$ and $x = 300$. — DNS; - - equation (38) with $\kappa = 0.41$ and $B = -7$; $\cdots u^+ = \frac{1}{0.41} \ln y^+ + 5.1$. b) SEP: Velocity profile at reattachment $x = 412$. — DNS; - - $u^p = \frac{1}{0.41} 2\sqrt{y^p} - 7$.

3.3.2. The overlap region

The laws presented in section 2.1.2 are compared with data from the simulations in figure 20. And the results from section 2.2 regarding the logarithmic region are presented in figure 21.

For APG1 the extended logarithmic law (18) gives profiles that are more in agreement than the usual ZPG logarithmic law, see figure 20a. However, the value of the additive constant B in equation (18), which has a value of -2 close to separation in both DNS and experiments, had to be set to $+1.5$ to fit the

DNS data in APG1. This is true for all streamwise positions, and hence the value of the additive constant seems to depend on the pressure gradient, and not the Reynolds number. In the attached region of separating boundary layer, the profile from equation (18) with $B = -2$ gives the best approximation, shown in figure 20b. This is in agreement with the earlier investigation of the flow just upstream of separation in the simulation of NM, see Skote & Henningson (1999).

The profiles in the separated region, figure 21a, are compared with the arctan law derived in section 2.2. The profile given by equation (38) is in much better agreement with DNS than the corresponding ZPG law, also shown in the figure. The additive constant is -7 for the separated case. It should also be noted that the extended logarithmic law derived for an attached layer under a strong APG, equation (18), gives a poor agreement with DNS data in the separated region (not shown in the figure). At the point of reattachment ($x = 412$) the profile is given in pressure gradient scaling in figure 21b. The asymptotic version of equation (39) is in good agreement with DNS data since u_τ is close to zero.

Thus, the conclusion is that the equations describing the overlap region derived in section 2 are in qualitative agreement with DNS data, and are far more consistent with DNS data than the corresponding ZPG laws.

However, due to the low Reynolds numbers, it is not possible to draw any definite conclusions regarding the overlap region. To properly clarify these matters, high Reynolds number data are required, and the experiments of Alving & Fernholz (1996) are therefore analyzed in section 4.

3.3.3. *The outer part*

As discussed earlier in section 2.1.3, there are many theories for describing the profiles in the outer part. All of these are at some point dependent on either experimental evidence or curve-fitting. An overall comparison and criticism of each of these theories is beyond the scope of the present investigation. In figure 22 the velocity profiles are plotted against the outer variable η for both cases but in different scalings. For APG1 the profiles collapse in the ZPG scaling despite the strong APG as seen in figure 22a. For the separated case in figure 22b, the profiles are shown in the pressure gradient scaling. The profiles are spread and do not collapse at all. However, the profiles collapse if plotted in the separated region and in the attached region separately, which is indicated with solid and dashed profiles. Thus, the profiles fall on a single curve if the distinction between the separated and attached region is made. However, since the viscous and pressure gradient velocity scales are almost constant throughout the boundary layer, the advantage with u_p over u_τ is confined to the point around separation or in a case where u_τ fluctuate more than u_p .

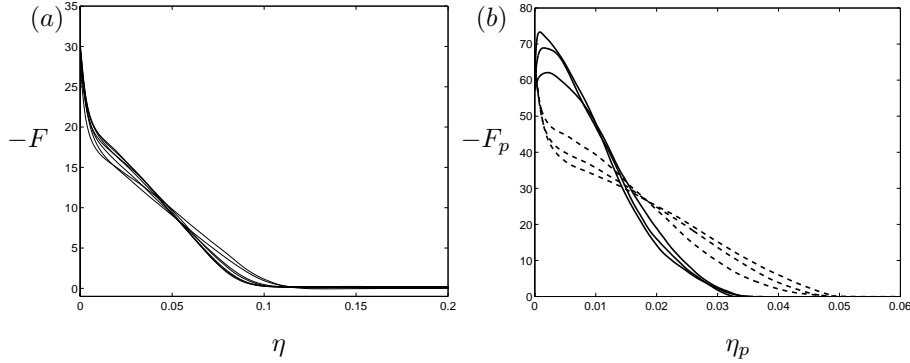


FIGURE 22. Velocity defect profiles at $x = 200 - 500$.
 a) APG1. b) SEP — $x = 250, x = 300$ and $x = 350$.
 - - $x = 450, x = 500$ and $x = 540$.

4. Discussion

In this section a comprehensive discussion about the relation between our results and others is presented.

4.1. Comparison with earlier DNS

The separated turbulent boundary layer simulated by DNS presented here has different characteristics compared to earlier DNS of a separation bubble. Efforts have earlier been made to create a bubble that starts and ends with a ZPG turbulent boundary layer. In the simulation presented here, the boundary layer is everywhere subject to an APG. To obtain a bubble with such a small extension in the streamwise direction as in the simulations of NM and SC, requires a strongly varying pressure gradient in order to force the boundary layer to separate and then reattach. The pressure gradient in those simulations was imposed by a strongly varying normal velocity at the freestream edge. This, in turn, creates a large normal gradient in the mean flow at the upper boundary. Here, the streamwise pressure gradient does not vary as rapidly as in the earlier DNS. However, the boundary layer reattaches upstream of the fringe region even if no favorable pressure gradient is applied. The variation of the normal velocity is much weaker than in NM, see figure 23. The freestream V varies approximately in the same way in SC as in NM.

The integrated quantities, such as the shape factor and momentum thickness, cannot be compared with data from earlier DNS of separated flow by SC and NM. This is due to the behavior of the velocity profiles at the freestream in those simulations. At some streamwise position the maximum value of u is located in the middle of the boundary layer, and the value at the upper boundary is three times lower. Figure 24 shows velocity profiles at the position of maximum back-flow from the three different simulations. The profiles from NM and SC show a considerable velocity gradient at the upper boundary, and

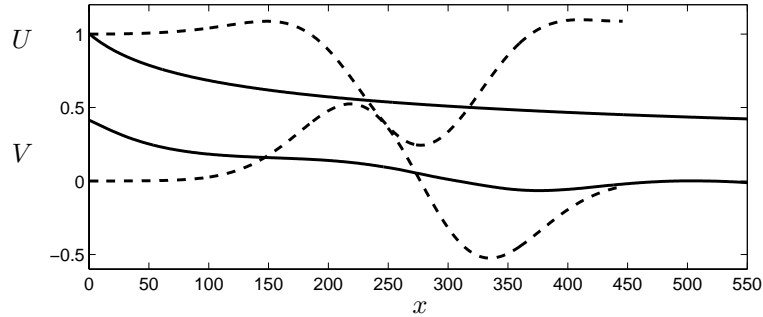


FIGURE 23. — V and U from SEP; - - V and U from NM. The profiles starting from unity is U .

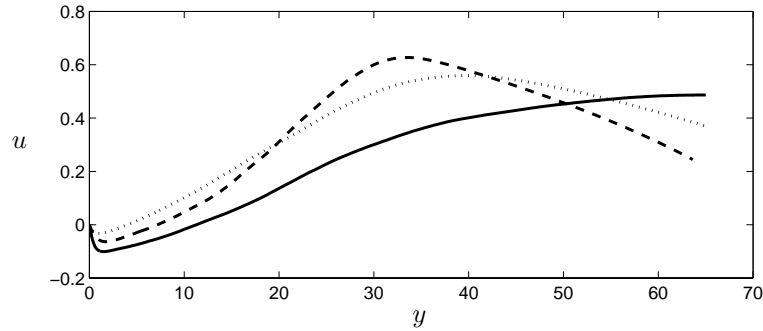


FIGURE 24. Velocity profiles. — from SEP; - - from NM; \cdots from SC.

the value at the upper boundary of U varies strongly in NM, as seen from figure 23. Here the x values have been recalculated in our simulation coordinates. However, the relative starting positions of the boundary layers cannot be calculated and is here matched by letting the starting points of all three simulations be located at $x = 0$. Furthermore, from figure 24 it is clear that the back-flow is stronger in the present simulation than in NM and SC.

The strong gradient at the freestream makes it difficult to define a boundary layer edge. In the simulation presented here, no such ambiguity about the boundary layer edge and thickness exists. Since there was no real freestream in SC and NM, the friction coefficient, C_f , was calculated with the value of unity for the freestream velocity U at all streamwise positions. Comparison of the C_f from NM and SC with our simulation is made in figure 25. It is clear from figure 25 that our separation bubble is longer than the other two. In figure 25 the C_f from our simulation has been calculated using the same technique as in NM and SC, i.e. with a value of unity for the freestream velocity.

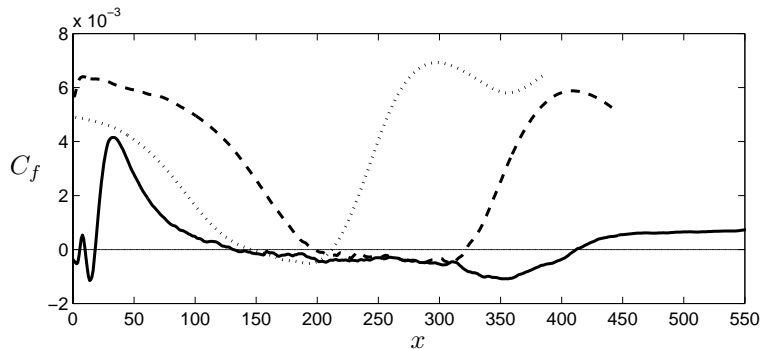


FIGURE 25. — C_f from SEP; - - C_f from NM; \cdots C_f from SC.

4.2. The overlap region in experiments

To further investigate the theoretical expressions from section 2.1.2, but at a larger Reynolds number than is possible to reach with DNS, the experimental data from Alving & Fernholz (1996, 1995) are investigated.

In the work of Alving & Fernholz (1995) the velocity profiles showed considerable departure from the law of the wall valid for ZPG flow. By using the Perry-Schofield coordinates, modified by Dengel & Fernholz (1990), the curves were forced to collapse. However, the procedure of determining the velocity scale a posteriori, from the collapsed velocity profiles, make the analysis less valuable. The measured profiles are here examined from the other standpoint, the extended law of the wall. In figure 26 the profiles before separation and in the separated region are shown. Upstream of separation the extended logarithmic law (18) with the standard value of -2 for the additive constant predicts the profiles well. In the separated region (only one profile available) the profile given by equation (38) gives a better prediction than equation (18). However, a change in the additive constant in equation (18) can make the agreement with the experimental profile equally good.

Thus, the experimental data of Alving & Fernholz confirm and strengthen the conclusion drawn from our DNS data in section 3.3.2.

4.3. Comparison with other theories for the overlap region

A number of investigators have, with different methods, tried to obtain the theoretical velocity profile in APG flows, corresponding to the logarithmic profile in a ZPG flow.

According to Tennekes & Lumley (1972), the scaling with the pressure gradient velocity u_p (with $u_\tau = 0$) should lead to the same form of matching as in the zero pressure gradient case. From this assumption a logarithmic law is obtained in the same manner as the usual procedure of matching the outer

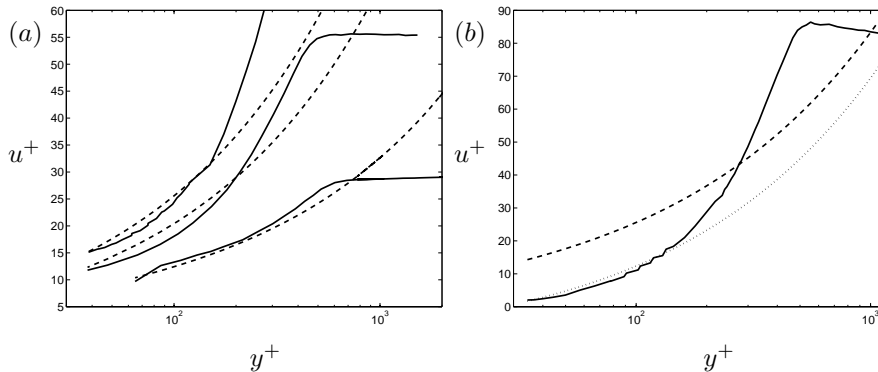


FIGURE 26. Experimental data from Alving & Fernholz (1995). a): Velocity profiles upstream of separation. - - equation (18) with $\kappa = 0.41$ and $B = -2$. b): Velocity profiles in the separated region. - - equation (18) with $\kappa = 0.41$ and $B = -2$. \cdots equation (38) with $\kappa = 0.41$ and $B = -7$.

and inner solutions. The log law becomes,

$$u^p = \frac{1}{\kappa} \ln(y^p) + B. \quad (45)$$

This is clearly wrong, since the scaling with u_p leads to the the half-power law, equation (20).

According to Stratford (1959), the velocity profile should be a half-power law close to separation. Also Yaglom (1979) showed that a dimensional analysis gives the following expression for the velocity profile close to separation,

$$u^+ = K^+ \sqrt{\lambda y^+} + K_1^+, \quad (46)$$

which can be expressed in pressure gradient scaling,

$$u^p = K \sqrt{y^p} + K_1. \quad (47)$$

Yaglom (1979) also proposed a fairly complicated dependence of K and K_1 on u_p and u_τ . This dependency was introduced to extend the theory valid at separation to the region upstream of detachment. It may not be regarded as a sound procedure to incorporate a functional behavior in constants of an expression valid only in an asymptotic state.

4.4. Alternative scaling of the back-flow

As suggested by Simpson (1983), the back-flow mean profiles may be scaled by the maximum mean back-flow velocity (u_N), together with the normal coordinate scaled with the distance from the wall to the maximum (N). The profiles scaled in this way are plotted in figure 27. Simpson (1983) also gives a logarithmic profile to be valid for $0.02 < y/N < 1.0$ with a constant A involved.

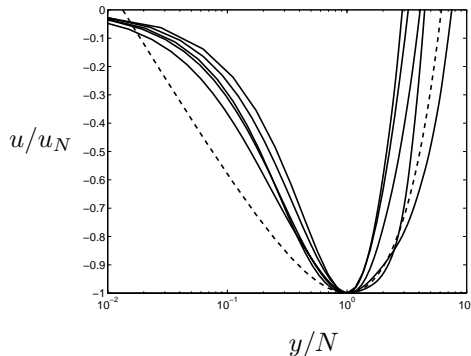


FIGURE 27. SEP: Velocity profiles at $x = 200$, $x = 250$, $x = 300$, $x = 350$ and $x = 400$. u_N and N are the maximum mean back-flow velocity and its distance from the wall. - - profile from equation (48)

$$\frac{u}{u_N} = A \left[\frac{y}{N} - \ln \left(\frac{y}{N} \right) - 1 \right] - 1. \quad (48)$$

The constant A has been given a number of different values in numerous experimental investigations by, e.g. Dianat & Castro (1989) and Devenport & Sutton (1991). Thus, the law seems to be of limited value. For comparison, the profile given by equation (48) is also shown in figure 27 with $A = 0.3$ as suggested by Simpson (1983). The collapse of the profiles is poor, and the agreement with equation (48) is as bad as in the DNS of a backward-facing step by Le *et al.* (1997).

5. Conclusion

Direct numerical simulations of two turbulent boundary layers have been performed. The flows are subject to slightly different adverse pressure gradients, resulting in two very different flows. One is everywhere attached while the other is separated. The case with separation still forms a boundary layer with a clearly defined freestream edge, distinguishing it from earlier attempts to simulate a separation bubble.

The near-wall flow was shown to be predicted by a straightforward analysis of the turbulent boundary layer equations. The theory is based on two different velocity scales easily extracted from the parameters of the flow. Thus, the theory is applicable to turbulence modelling. Furthermore, it was possible to extend the theory to the case of separation.

The velocity profile in the viscous sub-layer was shown to obey a law dependent on the pressure gradient, in both the attached and separated cases. A velocity profile for the overlap region was derived and showed better consistency with DNS data than the corresponding law of the wall for a zero pressure gradient boundary layer. In the attached boundary layer the overlap profile consists

of square-root and logarithmic parts, while in the separated region it consists of square-root and arc-tangents functions.

The near-wall streaks are weakened by the adverse pressure gradient, and the spacing in viscous units is reduced. In the separated case streaks reappeared in the region with strong back-flow. The turbulent structures convecting from the region upstream of separation are lifted above the separation bubble, and are weakened before reaching reattachment. The normal velocity towards the wall in the vicinity of reattachment show a tube-like structure, where also positive Reynolds shear stress results in destruction of turbulence energy.

Comparison with earlier DNS of separated turbulent boundary layers shows that the present simulation is well resolved and has a stronger and larger recirculation region.

Acknowledgments

Computer time was provided by the Center for Parallel Computers (PDC) at the Royal Institute of Technology (KTH), the National Supercomputer Center in Sweden (NSC) at Linköping University, and the National Aerospace Laboratory (NAL) in Tokyo.

In addition we thank Doctor Naoki Hirose and coworkers for the help with implementing the code on the Numerical Wind Tunnel.

We would also like to thank Doctor Erik Lindborg and Professor Arne Johansson for fruitful discussions and for their valuable comments on the manuscript.

References

- AFZAL, N. 1996 Wake layer in a turbulent boundary layer with pressure gradient: a new approach. In *IUTAM Symposium on Asymptotic Methods for Turbulent Shear flows at High Reynolds Numbers* (ed. K. Gersten), pp. 95–118. Kluwer Academic Publishers.
- ALVELIUS, K. & SKOTE, M. 2000 The performance of a spectral simulation code for turbulence on parallel computers with distributed memory. *Tech. Rep. TRITAMEK 2000:17*. Royal Institute of Technology, Stockholm.
- ALVING, A. E. & FERNHOLZ, H. H. 1995 Mean-velocity scaling in and around a mild, turbulent separation bubble. *Phys. Fluids* **7**, 1956–1969.
- ALVING, A. E. & FERNHOLZ, H. H. 1996 Turbulence measurements around a mild separation bubble and downstream of reattachment. *J. Fluid Mech.* **322**, 297–328.
- BRADSHAW, P. 1967 The turbulent structure of equilibrium boundary layers. *J. Fluid Mech.* **29**, 625–645.
- CEBECI, T. & SMITH, A. M. O. 1974 *Analysis of Turbulent Boundary Layers*. Academic Press.
- COLES, D. 1956 The law of the wake in the turbulent boundary layer. *J. Fluid Mech.* **1**, 191–226.

- DENGEL, P. & FERNHOLZ, H. H. 1990 An experimental investigation of an incompressible turbulent boundary layer in the vicinity of separation. *J. Fluid Mech.* **212**, 615–636.
- DEVENPORT, W. J. & SUTTON, E. P. 1991 Near-wall behavior of separated and reattaching flows. *AIAA J.* **29** (1), 25–31.
- DIANAT, M. & CASTRO, I. P. 1989 Measurements in separating boundary layers. *AIAA J.* **27** (6), 719–724.
- DRIVER, D. M. 1991 Reynolds shear stress measurements in a separated boundary layer flow. AIAA Paper 91-1787.
- DURBIN, P. A. & BELCHER, S. E. 1992 Scaling of adverse-pressure-gradient turbulent boundary layers. *J. Fluid Mech.* **238**, 699–722.
- HANCOCK, P. E. 2000 Low reynolds number two-dimensional separated and reattaching turbulent shear flow. *J. Fluid Mech.* **410**, 101–122.
- HENKES, R. A. W. M. 1998 Scaling of equilibrium boundary layers under adverse pressure gradient using turbulence models. *AIAA J.* **36**, 320–326.
- KADER, B. A. & YAGLOM, A. M. 1978 Similarity treatment of moving-equilibrium turbulent boundary layers in adverse pressure gradients. *J. Fluid Mech.* **89**, 305–342.
- LE, H., MOIN, P. & KIM, J. 1997 Direct numerical simulation of turbulent flow over a backward-facing step. *J. Fluid Mech.* **330**, 349–374.
- LUNDBLADH, A., BERLIN, S., SKOTE, M., HILDINGS, C., CHOI, J., KIM, J. & HENNINGSON, D. S. 1999 An efficient spectral method for simulation of incompressible flow over a flat plate. *Tech. Rep.* TRITA-MEK 1999:11. Royal Institute of Technology, Stockholm.
- MCDONALD, H. 1969 The effect of pressure gradient on the law of the wall in turbulent flow. *J. Fluid Mech.* **35**, 311–336.
- MELLOR, G. L. 1966 The effects of pressure gradients on turbulent flow near a smooth wall. *J. Fluid Mech.* **24**, 255–274.
- MELLOR, G. L. 1972 The large reynolds number, asymptotic theory of turbulent boundary layers. *Intl J. Engng Sci.* **10**, 851–873.
- MELNIK, R. E. 1989 An asymptotic theory of turbulent separation. *Computers & Fluids* **17**, 165–184.
- MUSKER, A. J. 1979 Explicit expression for the smooth wall velocity distribution in a turbulent boundary layer. *AIAA J.* **17**, 655–657.
- NA, Y. & MOIN, P. 1998a Direct numerical simulation of a separated turbulent boundary layer. *J. Fluid Mech.* **374**, 379–405.
- NA, Y. & MOIN, P. 1998b The structure of wall-pressure fluctuations in turbulent boundary layers with adverse pressure gradient and separation. *J. Fluid Mech.* **377**, 347–373.
- NORDSTRÖM, J., NORDIN, N. & HENNINGSON, D. S. 1999 The fringe region technique and the fourier method used in the direct numerical simulation of spatially evolving viscous flows. *SIAM J. Sci. Comp.* **20** (4), 1365–1393.
- PERRY, A. E. 1966 Turbulent boundary layers in decreasing adverse pressure gradients. *J. Fluid Mech.* **26**, 481–506.
- PERRY, A. E. & FAIRLIE, B. D. 1975 A study of turbulent boundary-layer separation and reattachment. *J. Fluid Mech.* **69**, 657–672.

- PERRY, A. E. & SCHOFIELD, W. H. 1973 Mean velocity and shear stress distributions in turbulent boundary layers. *Phys. Fluids* **16** (12), 2068–2074.
- ROTTA, J. C. 1962 Turbulent boundary layers in incompressible flow. *Prog. Aerospace Sci.* **2**, 3–219.
- SAMUEL, A. E. & JOUBERT, P. N. 1974 A boundary layer developing in an increasingly adverse pressure gradient. *J. Fluid Mech.* **66**, 481–505.
- SCHLICHTING, H. 1979 *Boundary layer theory*. McGraw-Hill.
- SCHOFIELD, W. H. 1981 Equilibrium boundary layers in moderate to strong adverse pressure gradients. *J. Fluid Mech.* **113**, 91–122.
- SIMPSON, R. L. 1983 A model for the backflow mean velocity profile. *AIAA J.* **21** (1), 142–143.
- SIMPSON, R. L. 1996 Aspects of turbulent boundary-layer separation. *Prog. Aerospace Sci.* **32**, 457–521.
- SIMPSON, R. L., CHEW, Y.-T. & SHIVAPRASAD, B. G. 1981*a* The structure of a separating turbulent boundary layer. part 1. mean flow and reynolds stresses. *J. Fluid Mech.* **113**, 23–51.
- SIMPSON, R. L., CHEW, Y.-T. & SHIVAPRASAD, B. G. 1981*b* The structure of a separating turbulent boundary layer. part 2. higher-order turbulence results. *J. Fluid Mech.* **113**, 53–73.
- SIMPSON, R. L., STRICKLAND, J. H. & BARR, P. W. 1977 Features of a separating turbulent boundary layer in the vicinity of separation. *J. Fluid Mech.* **79**, 553–594.
- SKÅRE, P. E. & KROGSTAD, P.-A. 1994 A turbulent equilibrium boundary layer near separation. *J. Fluid Mech.* **272**, 319–348.
- SKOTE, M., HENKES, R. A. W. M. & HENNINGSON, D. S. 1998 Direct numerical simulation of self-similar turbulent boundary layers in adverse pressure gradients. *Flow, Turbulence and Combustion* **60**, 47–85.
- SKOTE, M. & HENNINGSON, D. 1999 Analysis of the data base from a dns of a separating turbulent boundary layer. Center for Turbulence Research, Annual Research Briefs 1999, 225–237.
- SPALART, P. R. & COLEMAN, G. N. 1997 Numerical study of a separation bubble with heat transfer. *European J. Mechanics B/Fluids* **16**, 169.
- SPALART, P. R. & WATMUFF, J. H. 1993 Experimental and numerical study of a turbulent boundary layer with pressure gradients. *J. Fluid Mech.* **249**, 337–371.
- STRATFORD, B. S. 1959 The prediction of separation of the turbulent boundary layer. *J. Fluid Mech.* **5**, 1–16.
- TENNEKES, H. & LUMLEY, J. L. 1972 *A First Course in Turbulence*. The MIT Press.
- TOWNSEND, A. A. 1961 Equilibrium layers and wall turbulence. *J. Fluid Mech.* **11**, 97–120.
- YAGLOM, A. M. 1979 Similarity laws for constant-pressure and pressure-gradient turbulent wall flows. *Ann. Rev. Fluid Mech.* **11**, 505–40.
- YAJNIK, K. S. 1970 Asymptotic theory of turbulent shear flows. *J. Fluid Mech.* **42**, 411–427.